A Phased Array Approach to Rock Blasting

Final Technical Report

for the period of 9/30/03 to 7/1/06

written by

Leslie Gertsch and Jason Baird

submitted

7 August 2006

DOE Award Number DE-FC26-03NT41940

University of Missouri-Rolla
Rock Mechanics & Explosives Research Center
Rolla, MO 65401

Disclaimer

Abstract

A series of laboratory-scale simultaneous two-hole shots was performed in a rock simulant (mortar) to record the shock wave interference patterns produced in the material. The purpose of the project as a whole was to evaluate the usefulness of phased array techniques of blast design, using new high-precision delay technology. Despite high-speed photography, however, we were unable to detect the passage of the shock waves through the samples to determine how well they matched the expected interaction geometry. The follow-up mine-scale tests were therefore not conducted. Nevertheless, pattern analysis of the vectors that would be formed by positive interference of the shockwaves from multiple charges in an ideal continuous, homogeneous, isotropic medium indicate the potential for powerful control of blast design, given precise characterization of the target rock mass.

Table of Contents

List of Figures

List of Figures (continued)

List of Tables

Executive Summary

Introduction and Scope of Investigation

The goals of the project were to evaluate whether a phased array approach to rock blasting is possible using modern ultra-precise blast delays, and to begin to quantify how well this approach can improve rock fragmentation while lowering overall costs.

Blasting tests were planned at three scales from laboratory to large excavation blasts, interspersed with graphical and numerical modeling of expected results, and comparison with actual results. Following successful demonstration of the technique, it was planned to be publicized in the technical media, including demonstrations, leading up to commercialization.

Background and Literature Review

There has been interest in controlled directional focusing of blasting shockwaves for some time, based on the principles of superposition and wave interference. The state of time delay technology has been insufficient to bring it into being before now.

Sonic Velocity Measurement

The minimum size of mortar test blocks for laboratory testing was determined by measuring the sonic velocity of samples of the rock simulant used.

Shockwave Visualization Tests

Laboratory-scale tests were performed with blocks of mortar into each of which were drilled two holes. Small explosive charges were detonated in these holes while the blocks were sealed in a blast chamber and monitored by high-speed film.

Multiple examples of two block sizes were tested, but none of the film footage showed usable images of shockwaves passing through the blocks. This would have been necessary to determine if the waves were actually following the patterns predicted during simulation.

Alternative Methods of Monitoring Shockwaves

Adaptation of geotomographic techniques, sacrificial sensors of several types (resistor, photoelastic, photoelectronic), telecentric lens-assisted imaging, and digital high-speed imaging of the rock surface are possible methods for monitoring the interactions of shockwaves.

Simulation of Shockwave Interactions

Basic graphical and numerical analyses of the relationships between relative shot locations, delay timing, and positive interference vector orientation show how they combine to enable more precise “aiming” of the energy contained in blasts.

Conclusion

The principle of Phased Array Blasting still appears to have great potential for improving rock fragmentation and thereby energy efficiency in mining and excavation. The key is thorough, precise, and accurate knowledge of the spatial variation of the physical properties of the target rock mass. This approach will bring a much greater level of control to the blasting engineer.

Introduction

This final technical report discusses the activities of the project team during the entire project period of performance. In the interests of completeness, this includes the activities described in previous progress reports.

Phased arrays are a new approach to releasing explosive energy in space and time borrowed from antenna engineering that could allow the mining industry to utilize a much larger proportion of explosive energy constructively than previously possible. A phased array is a pattern of energy sources whose phase differences are designed to force the interacting energy waves to produce resultant vectors of constructive and destructive interference in desired directions and locations.

The study was planned to evaluate the applicability of a phased array approach to rock blasting, specifically whether it can achieve the following expectations, and with what energy intensity reductions:

- Better fragmentation – defined as a narrower size distribution, more appropriate aspect ratio, and/or better strength and durability of the resulting rock particles.
- More efficient fragmentation – defined as achieving the purpose of the blast, including meeting the needs of downstream processing (especially crushing and grinding), with less total energy input.
- More precise blast design – defined as achieving the purpose of the blast with less uncertainty, and less variation between the design and the as-shot blast.

This study was planned to contribute to better control of blasting for responsible emission and by-product management, and reduction of materials handling. If successful, phased array blasting will help improve fragmentation efficiency, reduce energy usage, reduce dust emission, and reduce environmental disturbance – Vision Goals toward which the mining industry is working.

Scope of Investigation

The study was planned to proceed in the following approximate order, with some tasks overlapping:

1. Literature review to learn from previous work.
2. Laboratory scale blast tests to confirm visual monitoring of shockwave interactions.
3. Graphical study of interaction geometry and the vectors of constructive interference produced.
4. Mine scale blast tests.
5. Numerical analysis of blast test results and comparison with expectations.
6. Large-scale blast tests.
7. Analysis of blast test results and comparison with expectations.
8. Dissemination of findings through presentations and technical journal papers.
9. Planning of future research to lead to commercialization of Phased Array Blasting.

Background

High efficiency blasting directs as much energy as possible into fragmentation:

$$E_{total} = E_{fragmentation} + E_{vibration} + E_{flyrock} + E_{other\ losses} \qquad \text{(where } E_x = \text{Energy into X)}$$

An energy efficient blast is one that results in optimal rock fragmentation, with low ground vibration and little flyrock. Ground vibration and flyrock motion expend explosive energy that could be applied instead to rock fracturing.

Since low efficiency blasting is one consequence of imprecise initiation timing, precise digital initiation creates more energy-efficient blasts. Previous work on digital initiation has focused primarily on improving current blasting practices. Controlling the interaction of the stress waves that radiate from each blast hole through precise initiation timing directs multiple stress waves to areas in the rock where improved fragmentation is desired. The same precision then controls where the stress waves interact, enhancing the stress levels in the rock and improving fragmentation without increasing vibration or flyrock significantly.

When more energy is directed into fragmentation, blasting will be improved in several ways:

- Reduced Ground Vibration
- Better Fragmentation
- Reduced Powder Factor
- Lower Energy Consumption (both Blasting and Crushing/Grinding)
- Less Fly Rock and Improved Safety

Real improvements likely can be made in blasting practice through the new paradigm of high efficiency blasting (Lewis and Pereira, 2003; Cunningham, 2004; Rosenstock, 2004; Rossmanith, 2003a).

Current rock blasting techniques create zones of uneven rock fragmentation within the rock body, before explosive gas pressurization acts on the fragmented rock to move it into the muck pile. This uneven fragmentation often results rock size distributions in the muck pile that range from dust to boulders. Even good drilling and blasting technique produces extreme fragmentation zones immediately around the blast holes, and poor fragmentation zones in regions approximately midway between the holes. Uneven fragmentation increases the energy consumed in comminution, due to requirements for auxiliary rock breaking, special haulage, and increased difficulty in mechanical milling operations to produce economically desirable rock and stone sizes. These zones of uneven fragmentation are caused by uneven blast stress distributions within the rock body, which cause uneven rock strains.

The uneven stress distributions result from many factors. Some of these factors are best explained as Real World effects: inhomogeneities within the rock mass, macroscopic geologic variations (joints, vugs, bedding, etc.), and imperfect drilling and blasting techniques. Accounting for these effects consumes a major portion of the education and training of drillers and blasters within the industry, and much effort and expense by industry is aimed at helping to perfect drilling and blasting technique through software and hardware improvements.

Other factors can be understood best by considering an Ideal World, where the rock mass is homogeneous, there are no geologic imperfections, and drill/blast technique is perfect. The factors in uneven fragmentation in this Ideal World concern acoustic (stress) wave thermodynamic attenuation by the rock mass, the need for placement of explosive charges in discrete blast holes instead of being continuously distributed throughout the mass, and stress wave interference with/amplification of other stress waves within the blast. The first two Ideal World factors are intractable problems, given the industry's capabilities. Learning how to adjust the remaining factor for the greatest blasting efficiency was the subject of this study.

The Energy and Radial Cracking Theories of Blasting

According to common elements of the energy (Cook, 1974) and radial cracking (Persson, 1994) theories of blasting, the blasting process causes precompression of the rock, motion of the rock burden, and then rock bursting. The concept of burden represents the rock along the line of least resistance from a blast hole to a free surface during blasting.

During rock mass precompression, stress waves produce compressive strains in the rock at normal powder factors[1]. The strains remain everywhere compressive until the stress waves begin to reflect from free surfaces at the burden distance from the blasthole(s). During reflection, tensile stresses first appear in the rock mass, and if the powder factor is higher than being considered herein, scabbing or spalling of the free surface may result. In optimized blasting, the average strain for precompressed rock in the mass exceeds the rock's tensile strain capability, ε_o, by at least a factor of two.

As the stress waves move through the rock, radial outflow of material accompanying the waves results in net motion of the rock burden away from the blast hole(s), resulting in a decreasing velocity distribution going away from the hole(s). A reasonable assumption is that about 10% of the explosive energy is used to pressurize the rock mass. The remaining 90% is used to accelerate the burden.

Rock bursting occurs during the burden acceleration phase of blasting. For rock to burst it must be preloaded in compression, uncoupled from the unblasted portion of the rock mass, and then the compressive strains within the rock must suddenly be converted into tensile strains with intensities greater than ε_o. This strain conversion is postulated to occur through a release-of-load mechanism, much like what happens when a compressed spring is uncoupled from its restraints. The release-of-load happens due to a readjustment of the rock particle velocity distribution. Initially, the radial outflow of material accompanying the outgoing compressive stress wave has a velocity distribution that decreases outward from the blast hole. When the blasted portion of the rock mass is suddenly decoupled from the remainder of the mass, the velocity distribution suddenly converts to a so-called expanding distribution, whereby the velocities increase with distance from the blast hole. The result of this release-of-load mechanism is that the rock mass is apparently pulled apart by an impulsive effect, one not related to release wave, tensile spalling-type fragmentation. It simply bursts.

Fragment Preconditioning

Rock size distribution and fragment strength within the muck pile are critical factors in mining costs, with the costs of digging and comminution falling off faster than the average size

[1] Powder factor is the ratio of explosive weight to weight or volume of rock fragmented.

of the rock fragments, as the size decreases. Muck pile rock size distribution and fragment strength are not only a function of the rock type, but also depend on blast wave loading of the rock mass before (from previous blasts) and during blasting of the rock mass.

Blast waves not only shatter rock, they also precondition it. Shattering is rock fragmentation by blasting, but preconditioning produces tiny fractures within the blasted rock. These tiny fractures make rock easier to dig and to crush. Experiments and field observation have shown that an increase in $\bar{\varepsilon}/|\varepsilon_o|$ (the ratio of average strain during precompression to the rock's tensile strain capability) not only decreases the average muck pile fragment size, but it also reduces the relative hardness of the fragments, making them easier to dig and to crush (Cook, 1974).

The two important aspects of blasting on fragmentation are seen and unseen. The size of fragments is the visible result of blast design, and is very important to the crushing operation. Overly coarse fragmentation reduces primary crusher throughput, leading to greater downtime for clearing crusher bridging and plugging, and it increases the load to secondary and tertiary crushing stages because there will be less undersize that can be split off to bypass these stages. In other words, the size distribution of blasted rock introduced to the primary crusher affects the feed size distributions throughout the crushing stages, affecting productivity and energy consumption through the plant.

The second effect of blasting, which is not directly visible, is microfracturing within fragments that tends to soften them, making them easier to break. This has benefits to productivity, energy expenditure, and wear of consumable items, and is usually referred to as "preconditioning" of the rock.

Therefore, in the process of optimizing blasting, two factors are preeminent: proper fragmentation distribution for crusher input, and preconditioning of individual fragments by internal fracturing. The first factor is now measurable directly, through image analysis techniques, while the second must be assessed through study of production, energy consumption and supply cost.

Productivity and energy consumption are of essential importance in determining crushing and grinding effectiveness. While there can be a certain synergism between the two factors, improvements in energy efficiency is the topic of this research.

Mines expend enormous amounts of energy; a substantial portion goes to crushing and grinding, with the greatest efficiency gains to be made in the area of grinding because of the tremendous particle size reduction that takes place. There is significant evidence that blasting does affect crushing and grinding results, and that large savings in cost can accrue (Eloranta, 1995; Paley and Kojovic, 2001). The role of microfractures is very important at the grinding stage, because the fragments become harder at each stage of sizing since the feed is smaller and there are fewer geologic and blast induced fractures present in the fragments.

Energy Consumption in Crushing and Grinding

The energy required to reduce ore fragments to their optimal separation size is large, and in some parts of the process most of the energy is dissipated as heat. In fact, grinding efficiency has been estimated to be as low as one percent (Hukki, 1975; Willis, 1988).

The energy requirements to reduce fragments from an 80% feed size to an 80% product size can be calculated, using the third theory of comminution as developed by Bond (1952) (Bond's third theory is used because the work index has been measured and reported for many rocks):

$$W = 10W_i\left(\frac{1}{P^5} - \frac{1}{F^5}\right)$$

Where: W = work input, kWh/ton

W_i = work index for the specific rock type, kWh/ton

P = 80% passing size of the product

F = 80% passing size of the feed

Using this relationship allows examination of the work input required for different feed sizes and the work indices in the stages of comminution. In this exposition, W_i is held constant throughout the stages, although it may, in fact, vary. Provided consistency is maintained, the trends in energy consumption and cost will be correct.

Literature Review

The literature search confirmed our initial premise that we should be able to improve stress wave interactions within a rock mass. Some salient items:

- From Sames (1995):

> "Ground vibration levels are generally predicted using equations such as the USBM equation. These equations give reasonable estimates of the level of vibration but are usually associated with a high standard deviation and a prediction of the effects of varying important blast design parameters such as delay sequencing, delay intervals and the number of blastholes is difficult.
>
> The *Seed Waveform Modeling Concept* as an additional approach is described. It is based on the measured vibration response of a single blasthole and the principle of superposition. Each charge is adjusted for varying charge weight, distance to the monitor location and degree of coupling. If not defined differently, the model uses stochastic simulation techniques to determine the firing time of each charge and the coupling factor.
>
> The vibration can be simulated in all three measured dimensions for varying delay intervals. The optimum delay interval can be determined based on the peak particle vibration or the frequency of the resulting waveform."

In other words, we are justified in measuring blast vibration (and shock) characteristics from one or two blastholes, then using superposition to extrapolate the results to many blastholes, so long as we account for charge weight, monitoring location, and coupling.

- From Mueller and Boehnke (2004):

  "On the one hand the presented new method for blast vibration prediction includes many of the traditional findings about the blast effects in rock masses and on the other hand it comprises the theoretical model of the momentum effect of a blast design. The factor charge per delay is no longer applied; it should to be reduced to the individual charge, ignited in a blasthole. Using the prediction in the practice of blasting leads to the following improvements:

  - The size of a blast design can be increased and planned as a multiple-row-blasting. The sequential timing is used progressive, obtuse-angled to the free face and with the cut from one side only.
  - It can be ignited electrically, electronically or non-electrically. The strength of delay timing used should be chosen below the own frequency of rock formation, to avoid resonances.
  - Using a correct geometrical arrangement while igniting several charges in one row simultaneously a better fragmentation can be accomplished without increasing vibrations.
  - The precision and reliability of vibration predictions was improved especially for the near-field. The retrospective calculation of data of peak particle velocity or strain will be possible without updating measurements.
  - It is possible to derive detailed statements from special predictions for individual buildings of complainants or problematical recording points, which cannot be disputed by law courts because of the statistics.
  - The vibration prediction can be worked out for blastings in all types of rock masses and it is statistically supported, physically verifiable and has the exact dimension."

  The authors are attempting to utilize momentum theory to predict vibrations, by measuring rock strains. Their relative success indicates that we should be able to utilize a similar measurement system.

- From Rossmanith (2003b):

  "In particular, the delay time, the wave speeds in the rock mass, the shape of the wave pulse and the acoustic impedance mismatch have become decisive parameters in advanced blasting. Utilizing the wave speed and wave shapes of detonations, large scale tests in various countries (Australia, Chile, etc.) have shown that optimal delay timing requires shorter delay times in conjunction with allowing for a wider drilling pattern and the use of a reduced amount of explosives, i.e. a lower powder factor. This seemingly contradictory arrangement is fully justified by using scientific principles in blasting, and converting blasting from an art to a scientific discipline."

  "When a blast-hole detonates a blast wave is radiated into the surrounding material. For a linear elastic material, theory and lab model tests show that this blasting-induced stress wave consists of a leading compressive pulse and a

trailing tensile pulse. The length of this wave depends on several factors: the type of explosive (brisant or non-brisant explosive) and the type of rock. The rock mass takes into account the structural geology which is one of the controlling factors in blasting and fragmentation. The length of such a wave varies between a few meters and can be as long as 150 meters (492 ft.) in granite bedrock. The character and magnitude of the tensile tail strongly depends on the structure of the rock mass and, in a highly jointed rock mass, it may completely be absent. The wave speed (not the particle velocity!) varies between 2000m/s (6560fps) (soft sandstone) and 6,500m/s (21,320fps) (basalt and granite). Considering two adjacent blast-holes (Yamamoto et al. 1999), maximum fragmentation is achieved in those sections between the blast-holes, where the two tensile trailing sections of the blast waves meet. For simultaneously detonating charges this happens at the midsection of the spacing of these blast-holes; for a delayed charge it occurs off-centerline. Time-wise, this normally occurs within the range of a few milliseconds, hence, the inter-hole delay time must be chosen appropriately. In order to make full use of the adjacent rows, a considerably shorter delay time is chosen than in conventional blasting in order to exploit the superposition effect of the stress waves. However, care must still be taken, as the rock material in the leading row must move before the stress waves of the adjacent row arrive in order to find a free face. Again, the delay times can considerably be shortened as compared to conventional blasting. Optimal fragmentation has been achieved in all applications with electronic detonators, particularly in Chuquicamata in Chile, in various open-pit mines in the Hunter Valley in Australia and elsewhere, with an inter-row delay of between 16 to 25 milliseconds. The presence of one or several joint sets and faults is still a problem and wave propagation theory has to be merged with structural geology. The blast design must take into account the presence of the structural geological features and delay times must be altered according to the quality of the joints and faults and the thickness, orientation and quality of the rock layers in the rock mass. Unfortunately, in most cases the characterization of joints and faults, i.e. the identification of their position and the properties, remains highly incomplete and this situation renders the appropriate execution very difficult if not impossible at present. A third important quantity is the acoustic impedance, which is the product of wave propagation velocity and density of the rock. Again, previously, this parameter was not an ultimate necessity for achieving good fragmentation. Theory shows, that not only the acoustic impedance of the explosive (= product of velocity of detonation times the density of the explosive) is important, but even more so the ratio between the impedances between explosives and rock and between two types of rock in stratified rock. All of the following can basically be treated by using computational mechanics methods, i.e. by using more or less sophisticated computer software packages which feature dynamic codes based on either finite elements or some other numerical method. This would allow the user to highly extend the method to include non-linear material behaviour and introduce into the analysis the effects of geological structure as well as other additional complexities."

In this paper and the next (below), Rossmanith hints at the subject of our research when he discusses the interactions of the "tensile tails" of the blast waves. He seems confident that computational methods sophisticated enough to incorporate some structural geology factors will be able to predict the drill and blast parameters necessary to optimize the interactions of blast waves for the desired fragmentation effects.

- From Rossmanith (2004):

  "Under such conditions the stress waves produced by blasting very quickly dissipate in the rock mass and often their energy cannot effectively be put to work. This contribution shows the effect of open and closed joints – and to some degree also faulting – on the blast wave field and shows the influence of structural geology on the blasting result."

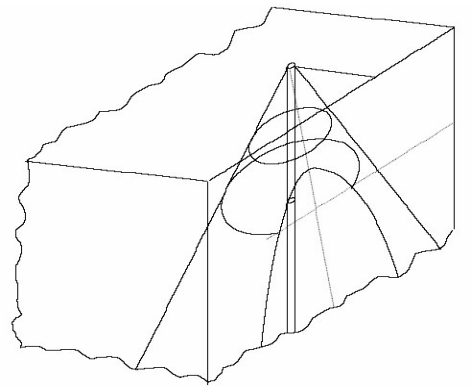

Figure 1. Supersonic bottom-initiated detonation of an explosive column charge showing the radiation of conical P and S waves and their reflection at the free face, from Rossmanith (2004).

Sonic Velocity Measurement

Precise knowledge of the shock wave velocity in the rock simulant used was crucial for accurate dimensioning of the samples. If the samples are too small, the shock wave interference effects that are the focus of the study cannot be monitored, and if the samples are too large, handling them inside the blast chamber becomes difficult or impossible. A search of the published literature located a mixed bag of values, some with information on material preparation, but most without. The range of sonic velocities (see below) is large enough that it was decided, instead, to fabricate samples of a convenient simulant (mortar) and measure their sonic velocities directly, after the samples cured. Then samples of dimensions suitable for blast tests were made of the same material.

- Chiang and Chen (2001) argued for the use of concrete reference specimens for calibrating ultrasonic pulse velocity equipment. Their specimens were 30cm×30cm×15cm (11.8 in.×11.8 in.×5.9 in.) in size. The weight ratio of cement/water/fine aggregate (dry)/coarse aggregate (dry) was 1.00/0.58/2.31/3.16. The specimens were cast and cured for one day in the mold, followed by 28 days in water. The average compressive strength was 20.7 MPa (3000 psi), and the pulse velocity median was **2981** m/s while the mean was **3117** m/s.
- Rösch *et al*. (1993) obtained cores taken from concrete columns in a building (fabrication details unknown), and measured both the uniaxial compressive strength and pulse velocity.

  Table 1. Results from Rösch *et al*. (1993).

Pulse Velocity in m/s	Compressive Strength in N/mm^2
3650	16.3
3890	27.7
4070	30.1
4120	37.2
4030	33.3
4180	41.5
4340	47.3

- The base concrete mixed for a study by Reinhardt and Grosse (1996) was reported as shown in Table 2, and then was modified in various ways as shown in Figures 2 through 6.

  Table 2. Components of samples from Reinhardt and Grosse (1996).

Component	Mass (kg/m^3)
Cement CEM 32.5 R	320.0
Aggregates0/2 mm t	635.3
2-8 mm	610.7
8-16 mm	531.9
Water	176.0

  This is the reference mix; the water-cement ratio is 0.55 and its cube compressive strength at 28 days is 25 MPa (3,626 psi). The non-reference mixes shown in the five charts below included various retarders; all apparently were tested at various water:cement ratios. The figures below illustrate the increase in strength with curing, as well as other parameters.

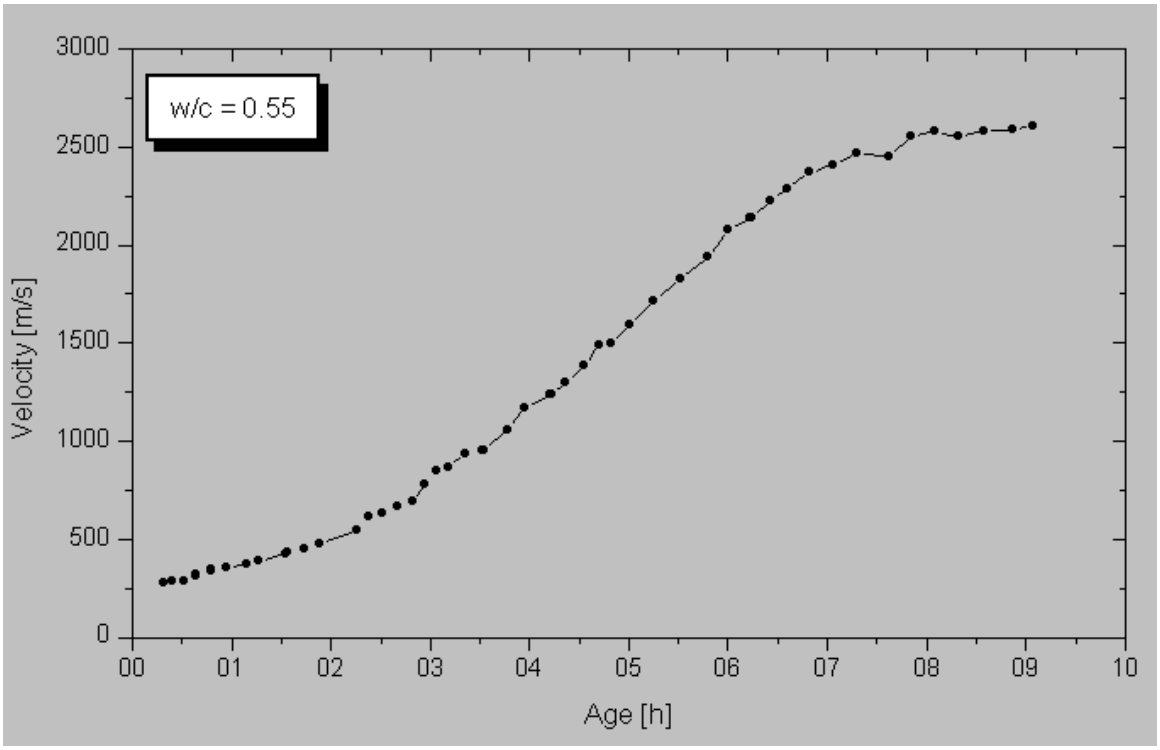

Figure 2. P-wave velocity of concrete as a function of length of cure, from Reinhardt and Grosse (1996).

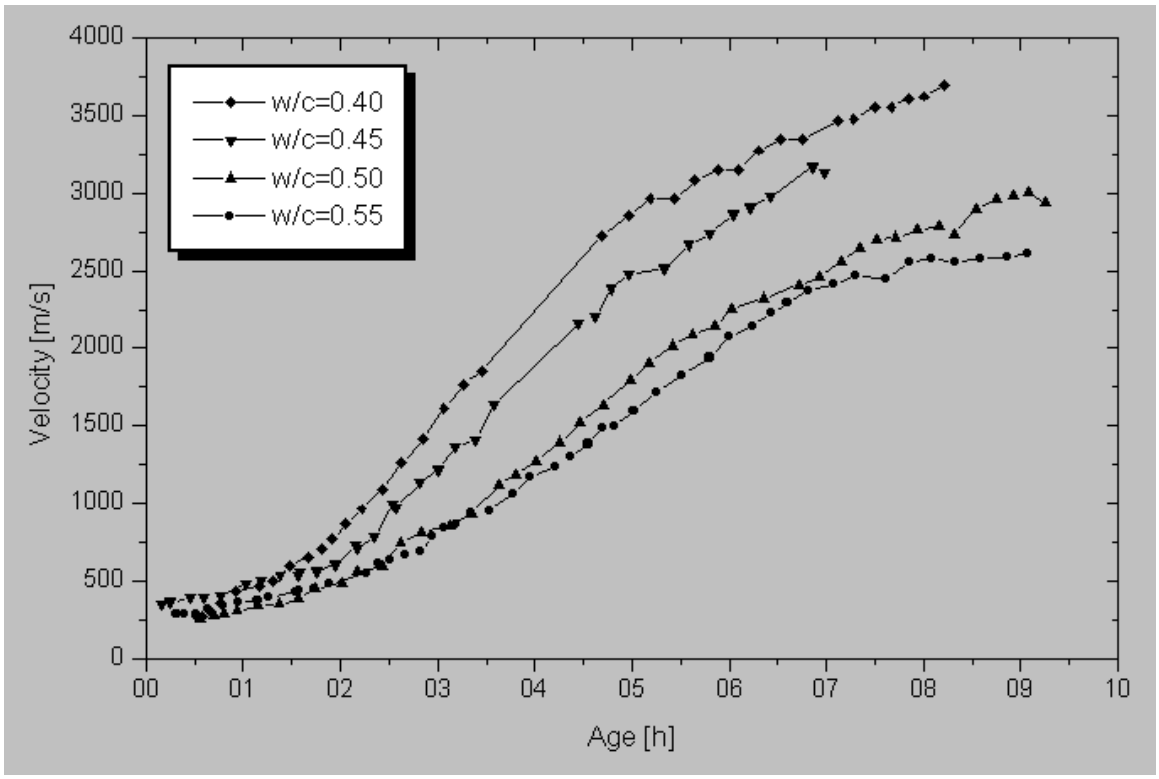

Figure 3. P-wave velocity of concrete as a function of age and water/cement ratio, from Reinhardt and Grosse (1996).

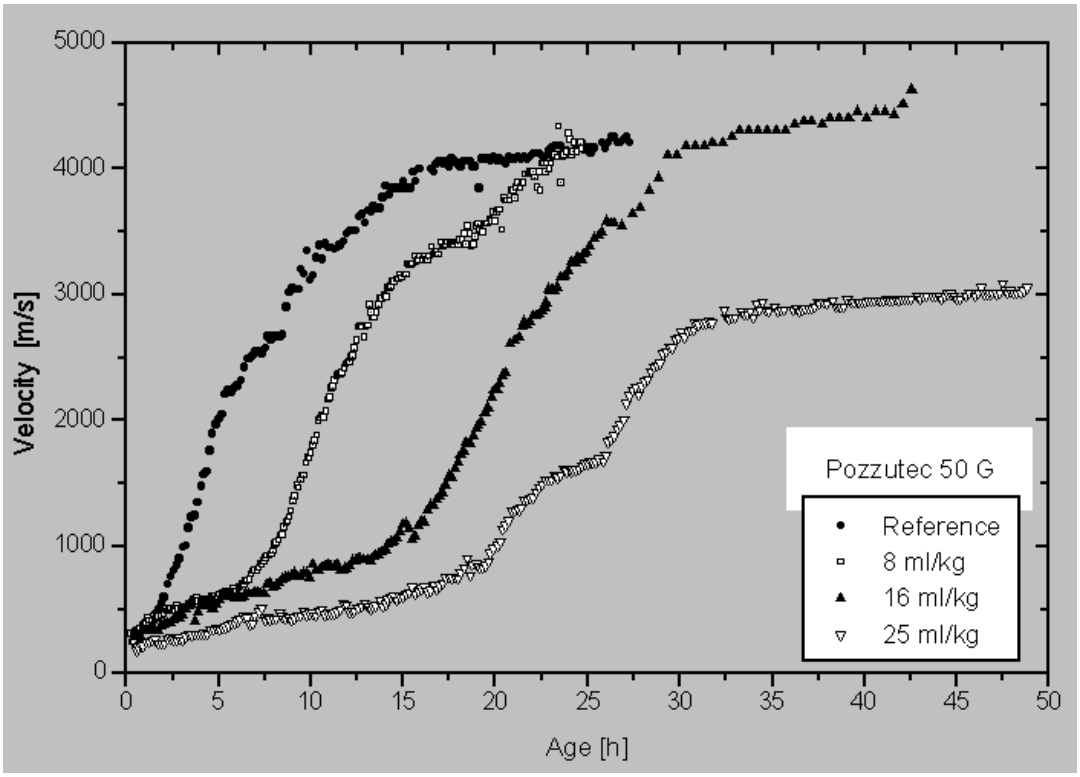

Figure 4. P-wave velocity of concrete as a function of the amount of Pozzutec retarder added, from Reinhardt and Grosse (1996).

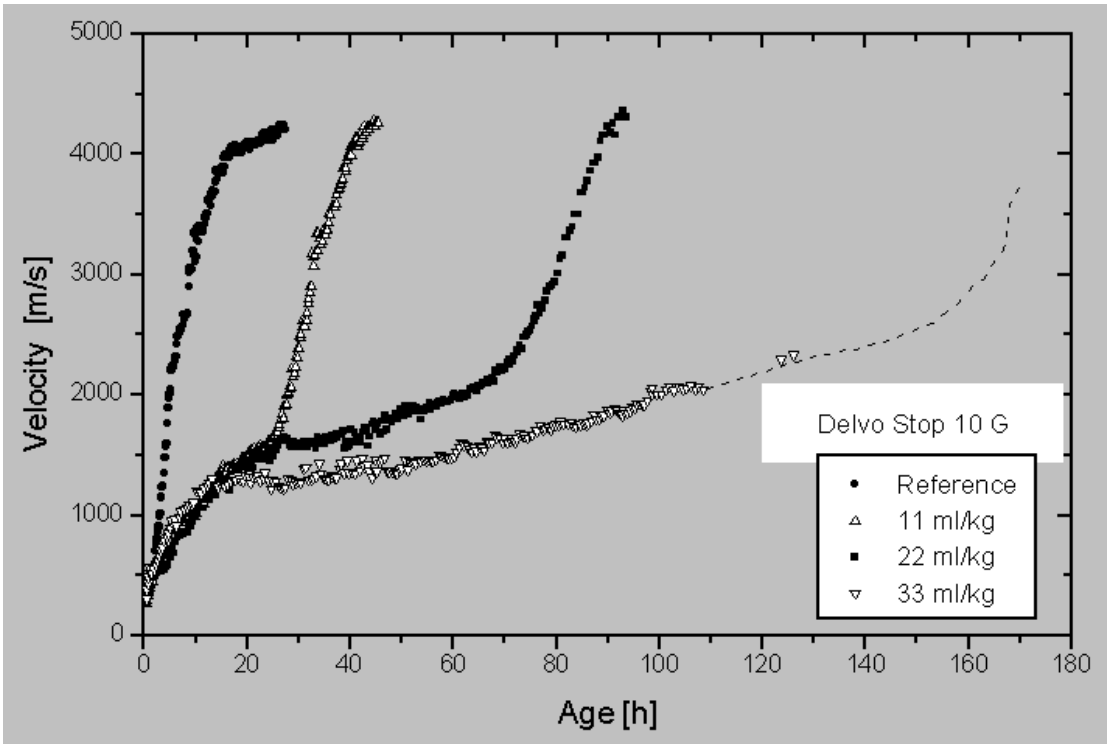

Figure 5. P-wave velocity of concrete as a function of the amount of Delvo Stop retarder added, from Reinhardt and Grosse (1996).

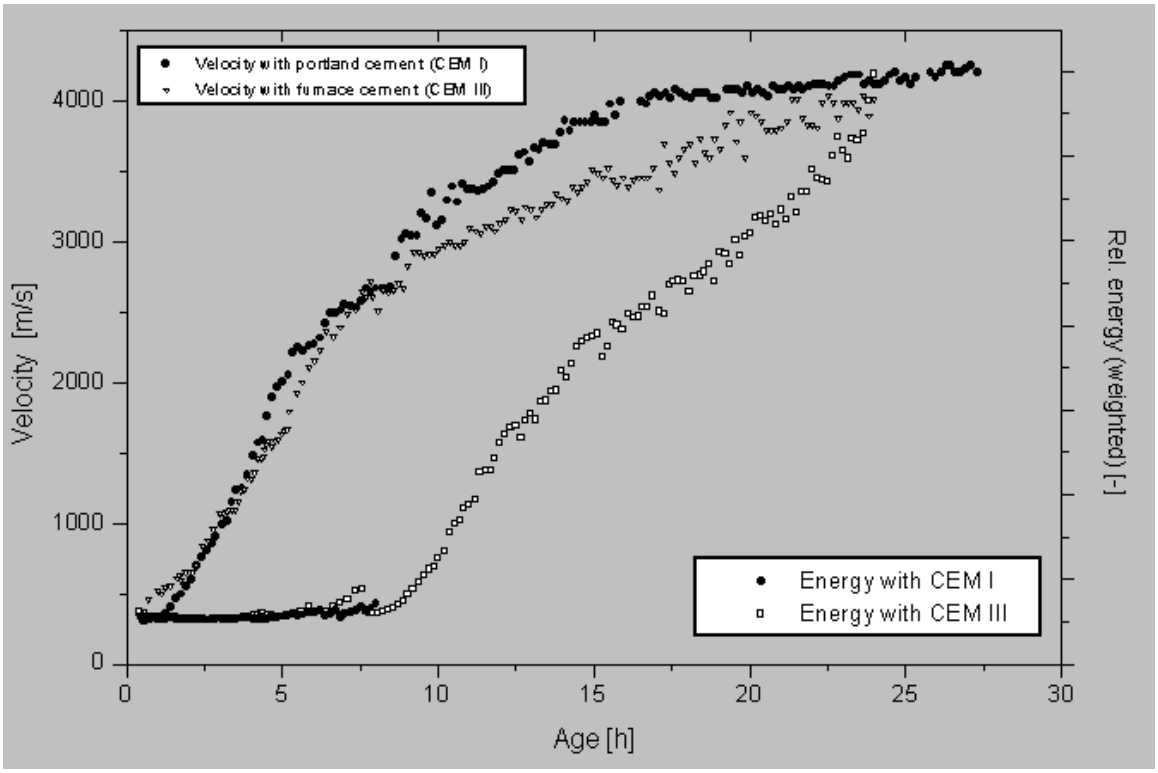

Figure 6. P-wave velocity of concrete as a function of cement components, from Reinhardt and Grosse (1996).

- Feldman (1977) outlined nondestructive techniques for testing concrete quality. Again, no definition of conditions or material components/fabrication procedures was provided.

Table 3. From Feldman (1977) and Leslie and Cheeseman (1949).

General Conditions	Pulse Velocity ft/sec (m/s)
Excellent	Above 15,000 (**4,615**)
Good	12,000-15,000 (**3,690**-4,615)
Questionable	10,000-12,000 (**3,080**-3,690)
Poor	7,000-10,000 (**2,150**-3,080)
Very Poor	Below 7,000 (**2,150**)

- In Figure 7, from a study by Kawahigashi (2001) on ways to improve concrete resistance to degradation by sea water, the data symbols themselves are larger than the precision required here. This reference did not prove useful for this study.

Table 4. Parameters of the concrete samples used by Kawahigashi (2001).

Materials of concrete	Cement: Blast-furnace slag cement (B-type) Aggregate: River aggregate (Gmax.: 25 mm, F.M.: 6.88, ρ: 2.64), river sand (F.M.: 2.90, ρ: 2.59)
Mix proportions	Water-cement ratio (W/C): 0.60 and 0.40 Unit water weight: 150 kg/m^3 Unit cement weight: 250 kg/m^3 (0.60) and 375 kg/m^3 (0.40) Air volume: 6±0.5 % Slump: 6 cm

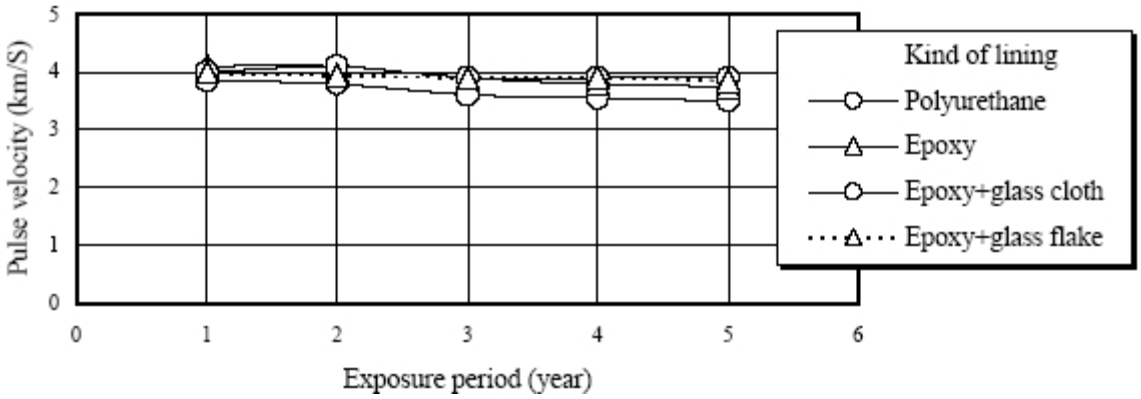

Figure 7. P-wave velocity of concrete as a function of length of exposure to salt water and to type of reinforcement, from Kawahigashi (2001).

Four preliminary samples were cast in the bottoms of milk cartons in order to measure the sonic velocity of concrete, utilizing QuikCrete brand "Mason Mix" with a volumetric ratio of 3.5 parts mortar mix to one part water at room temperature (Figure 8). The samples were covered with polyethylene bags and set aside to cure at room temperature. After five days, the poly bags were removed and the samples were allowed to continue curing at room temperature for an additional 23 days. The sample dimensions were approximately 10 x 10 x 7.6 cm (4 x 4 x 3 in.).

Figure 8. Preliminary mortar samples, after removal from molds.

Figure 9. Preliminary mortar samples, after face machining.

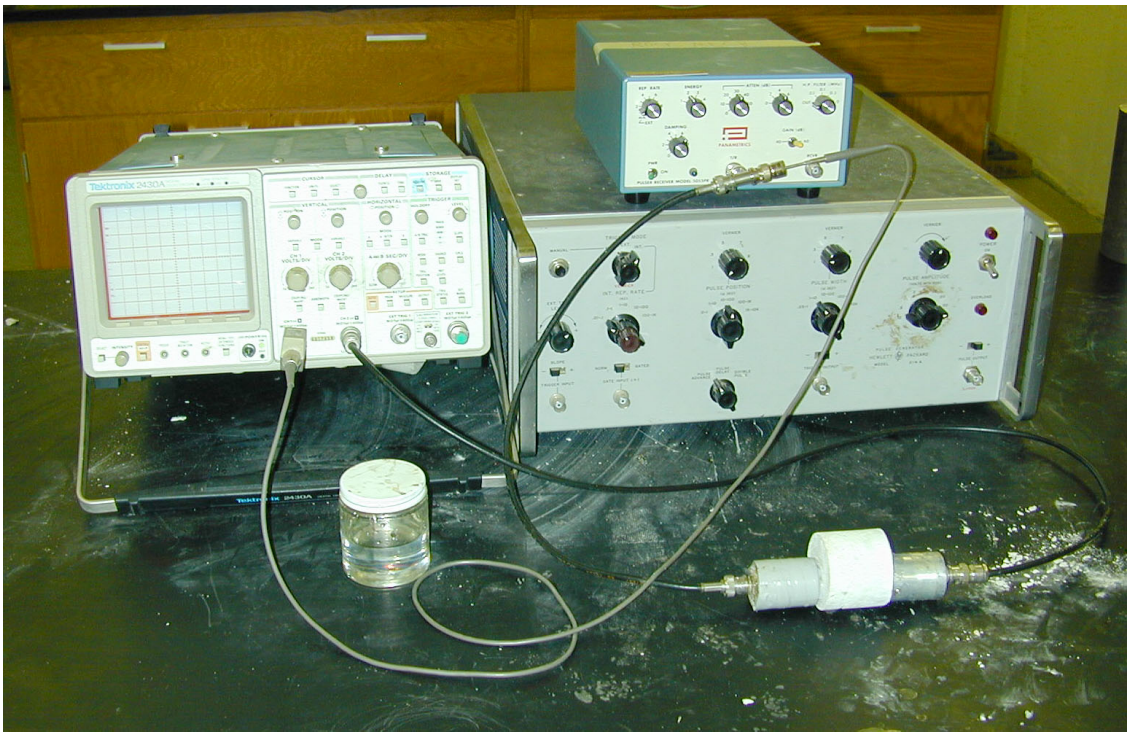

Figure 10. The ultrasonic pulse velocity measurement setup.

After the preliminary samples had cured, lab personnel utilized a wet saw to cut two faces into each sample for sonic velocity measurement per ASTM D2845-00 (Figure 9). The specification required face flatness to within 0.001 in., and face parallelism to within 0.004 in. for each 0.8 in. of lateral dimension. The samples were left at room temperature and humidity overnight after machining, and then measured for face flatness and parallelism. Each sample passed face flatness specification requirements; two out of the eight total parallelism measurements were out of specification by 0.0007 in., so sonic velocity tests for those faces were conducted but used for comparison purposes only.

The sonic velocities of the mortar samples were measured using the equipment shown in Figure 10. This is a standard setup for measuring the compressive (P) and shear (S) wave velocities of rock samples. P waves are faster than the S waves, which in turn are faster than surface (L) waves, and therefore the P waves constrain the minimum size of the mortar blocks. The setup consisted of a pulse generator, P- and S-wave sources, a digital oscilloscope, and cables in the appropriate configuration to send the pulse simultaneously to the wave generator and to the oscilloscope. The wave generator creates a sonic wave that travels through the target material (here illustrated by a core sample) and is picked up by the receiver. Comparison of the pulse transmitted by the wave receiver with the pulse sent directly to the oscilloscope permits measurement of the wave travel time through the material. Table 5 lists the measurements and calculated velocities from testing of the mortar samples.

Shockwave Visualization Tests

The sonic velocity data enabled the design and fabrication of appropriately sized mortar blocks for testing. Based on the data, 2.5-cm (1-in.) hole spacing should allow for up to four microseconds after detonation of explosives in the holes before the compressive waves from the detonation event collide between the holes. With each hole equidistant from its respective side face, up to 16 microseconds would pass before compressive waves from the detonation would reach the side faces and reflect. We estimated that this interval would allow time to capture indications of shock wave passage by recording the event with the Cordin framing camera at a rate of either ½ or 1 million frames per second. Initiation of the blasts was by precision exploding bridgewire (EBW) detonators with a total system jitter of 0.5 microseconds. The resulting images were examined for evidence of P, S, and L waves and their interactions.

We shot each visualization test in a disposable sample box designed to hold the mortar block securely in the correct position with relation to the viewing window. Each box contained an illuminating flash tube array below the viewing window (Figures 11 and 12). The boxes also contained a helium atmosphere to prevent fogging of our photographs due to luminescence that occurs when an explosive shock passes through an atmosphere containing nitrogen.

Each test in the blast chamber followed the same sequence. The sample in its box was sealed within the blast chamber (Figure 11), and the explosive initiator was tied in (Figure 12). The high-speed Cordin camera (Figure 13) was loaded with film and readied with a mirror transmitting the view from a porthole in the side of the blast chamber. This geometry prevented damage to the Cordin camera if the porthole were to blow out. Following this, the explosive charge within the block was connected to the initiating system.

Table 5. Sonic pulse velocity results for the preliminary mortar samples. The overall averages velocities are 3.198 mm/μsec (P-wave) and 0.079 mm/μsec (S-wave).

Block	Face	Dist 1	Dist 2	Avg Dist	P wave time	P velocity	P velocity	Velocity diff, face to face	S wave time	S velocity	S velocity	Velocity diff, face to face	Average velocities P wave	P wave	S wave	S wave
		in.	in.	in.	μsec	in/μsec	mm/μsec		μsec	in/μsec	mm/μsec		in/μsec	mm/μsec	in/μsec	mm/μsec
1																
	4"	5.548	5.560	5.554	44.0	0.126	3.206		72.0	0.077	1.959		0.125	3.167	0.077	1.967
	3" *	5.180	5.163	5.172	42.0	0.123	3.128		66.5	0.078	1.975					
2								0.079				0.016				
	3" (1)	5.688	5.676	5.682	45.0	0.126	3.207		70.0	0.081	2.062		0.128	3.254	0.081	2.068
	3" (2)	5.722	5.715	5.719	44.0	0.130	3.301		70.0	0.082	2.075					
3								0.094				0.013				
	4"	5.630	5.648	5.639	46.0	0.123	3.114		74.0	0.076	1.936		0.123	3.127	0.078	1.979
	3" *	5.804	5.821	5.813	47.0	0.124	3.141		73.0	0.080	2.022					
4								0.028				0.087				
	3" (1)	5.823	5.819	5.821	45.5	0.128	3.250		73.0	0.080	2.025		0.128	3.242	0.080	2.044
	3" (2)	5.596	5.611	5.604	44.0	0.127	3.235		69.0	0.081	2.063					
								0.015				0.037				

* faces did not meet parallelism specification

After the shot, the fragments of the sample and its box were gathered and the blast chamber was cleaned out. The film from the Cordin camera was unloaded and sent to a processing lab. The images reproduced in this report are digitized from the resulting prints.

Figure 11. A test sample being loaded (left) and sealed (right) in the blast chamber.

Figure 12. A test sample in its box with the flash array (left), and tied in to the initiator (yellow cord).

Figure 13. Setting up the high-speed camera.

Small Block Tests

Test 1

The explosive charge for the first test was 50 grain/ft det cord, the diameter of which allowed lab personnel to set the charges by drilling ¼ - in. holes, 1 ½ - in. deep at 1 in. spacing. Each of the two explosive charges was a five-in. length of det cord grouted into its respective hole in the sample, with the tag ends of the det cord left hanging for attachment to the EBW detonator (Figure 14). Attaching the tag ends together and tying-in the detonator so that exactly the same length of det cord separated each hole from the detonator would allow for shooting each hole at the same moment in time.

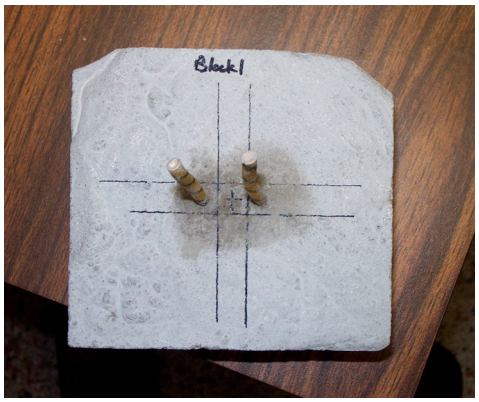

Figure 14. Test Sample 1 prior to the shot.

To initiate the shot, lab personnel used an RISI RP-501 EBW with the delay timing set so that the photography would start a few microseconds prior to detonation. A disposable array of 10 one-in. flash lamps illuminated the sample, with the illumination time regulated to avoid re-writing or over-exposing the film in the Cordin camera. For this first test, we decided to run the camera at ½ million frames per second, so that we could record for twice as long as would be possible with a recording rate of a million frames per second. Our framing camera uses 35 mm color film, and is limited to 26 frames.

The shot fired successfully, but the photography results were disappointing because black smoke from the tag end portions of the explosive charge obscured the view of the test sample surface (Figure 15). As a result of the obscuration, we ran the next test with an EBW as the explosive charge imbedded in each of the holes in the sample rather than using det cord as the explosive. As a possible aid to the research, lab personnel attempted to reconstruct each block after testing.

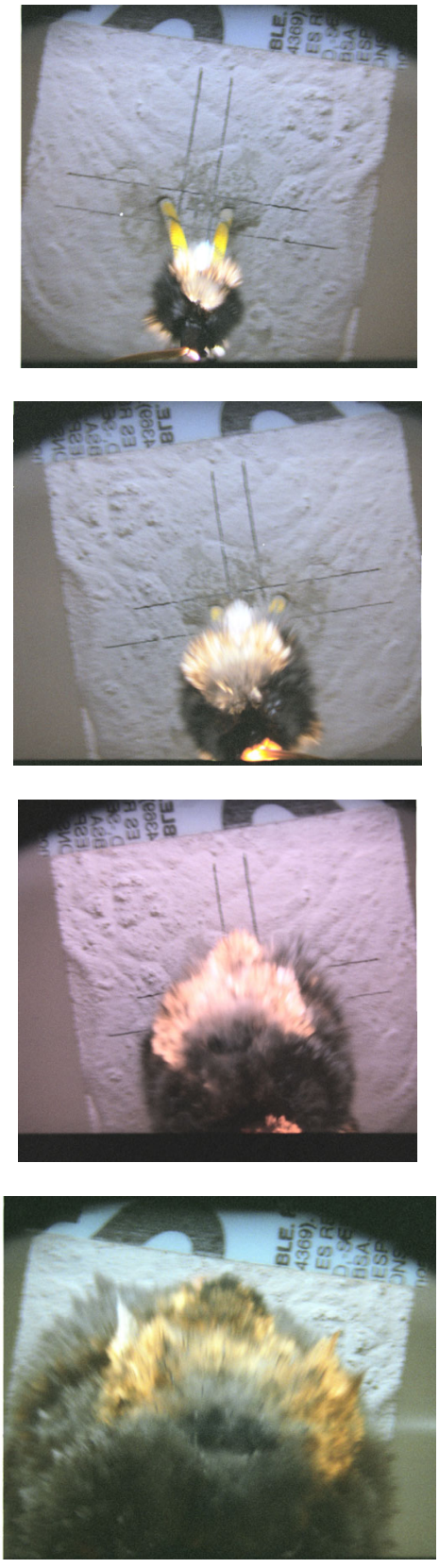

Figure 15. Selected frames from Test 1. View from top down.

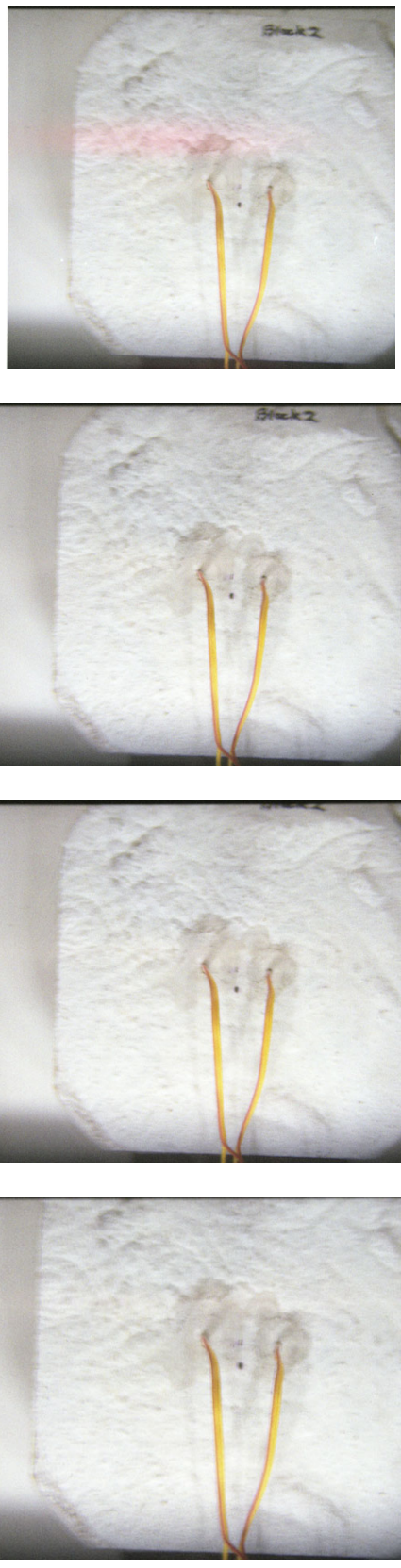

Figure 17. Selected frames from Test 2. View from top down.

Test 2

For this test, lab personnel bored two 0.95 cm (0.375 in.) diameter holes, 3.2 cm (1.25 in.) deep in the sample at 2.5 cm (1 in.) spacing, and grouted an RP-501 EBW detonator into each of the holes using the mortar mix (Figure 16). The explosive charge in each RP-501 was slightly less than 0.5 gram. With the maximum jitter in the system of 0.5 microsecond, the gross timing mismatch between the EBW's would be one microsecond but still precise enough to cause stress wave collision between the holes. So, using two separate EBW's would not give us the same timing precision for each hole charge firing as using the det cord arrangement from Test 1, but we judged the precision would be sufficient.

Figure 16. Test Sample 2, seen through the holding box viewing window.

Once again, we ran the Cordin camera at one frame per two μsec (½ million frames per second), and used a ten flashtube array for illumination during the shot.

This time, no black smoke obscured the block in the photographs (Figure 17), but we could see no indication of shock activity in the block. We assumed that the shock passage through the block material would cause some disruption of the surface, but none was evident.

For the next test, we positioned the block at a different angle so that surface movement should be visible on the photographs.

Test 3

For this test, in addition to changing the viewing angle for the photography, we buried the detonators only to their tops (about 2.0 cm or 0.8 in. deep) so that the explosive charges would be closer to the block surface. We hoped to be able to see any spallation or movement of the top surface.

Lab personnel bored two holes 2.5 cm (1 in.) apart, and each hole was 1.3 cm (0.5 in.) from the center of the block; they then grouted an RP-501 into each of the holes using the mortar mix. The detonator timing was set so the first photograph frame would be about 4μsec after the detonators fired.

The shot went well, with no obscuration due to smoke (Figure 18). The photos were a bit blurred, leading us to believe either that the camera focus needed readjustment, or that the detonation moved the block enough to blur the photos.

Test 4

This test was an attempt to photograph a block in the same manner as in Test 3, but with the block held rigidly in its mounting to prevent its movement during the shot. All of the other test parameters were the same, including a check of the camera focus by two different lab personnel.

The shot went well, with no obscuration due to smoke, though the photos were still a bit blurred (Figure 19). At this point, we decided to perform an extensive set of tests using photographic runs taking pictures of an array of focusing pins to check the focal point of the Cordin system.

This is necessary because the design of a framing camera of the Cordin sort does not allow viewing of the focus through the field lenses of the camera. It is possible for the shock of explosive detonations ringing the camera to change the set-up of the field lenses. Therefore, the only way to check the focus for each frame is to photograph a known set of pins at different distances to discover the actual focal length of each field lens. We discovered that the focus was best, for most of the frames, at the pin 1 in. behind the intended focal point.

We also increased the camera speed to 1 million frames per second (1 frame per microsecond), in hopes of reducing blurring in the photos by reducing the exposure and interframe times.

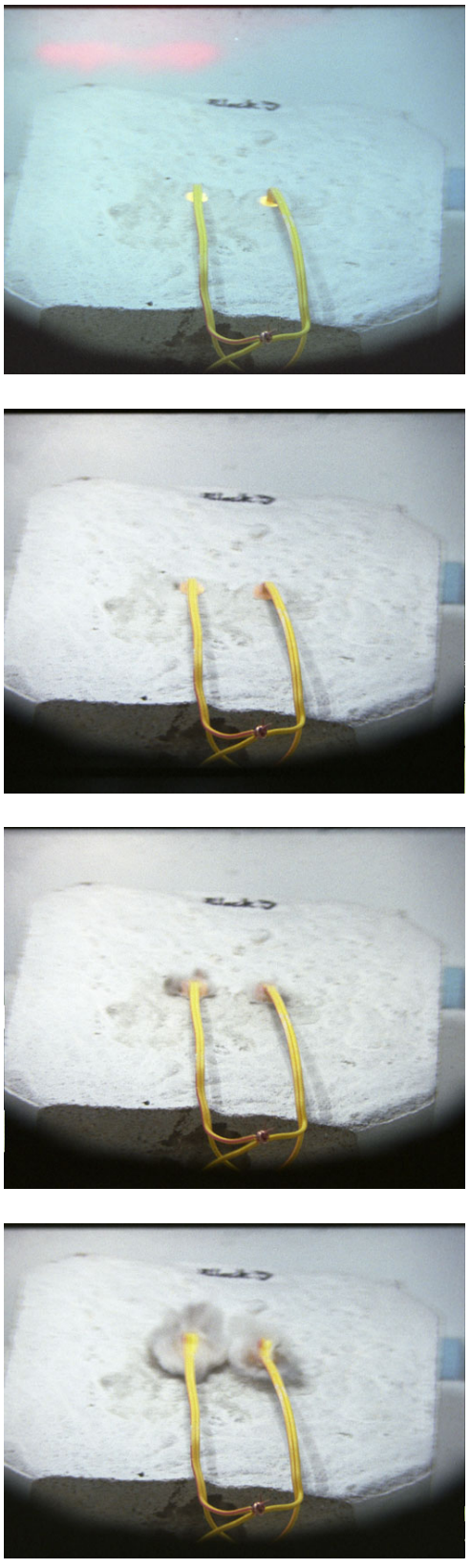

Figure 18. Selected frames from Test 3. View from top down.

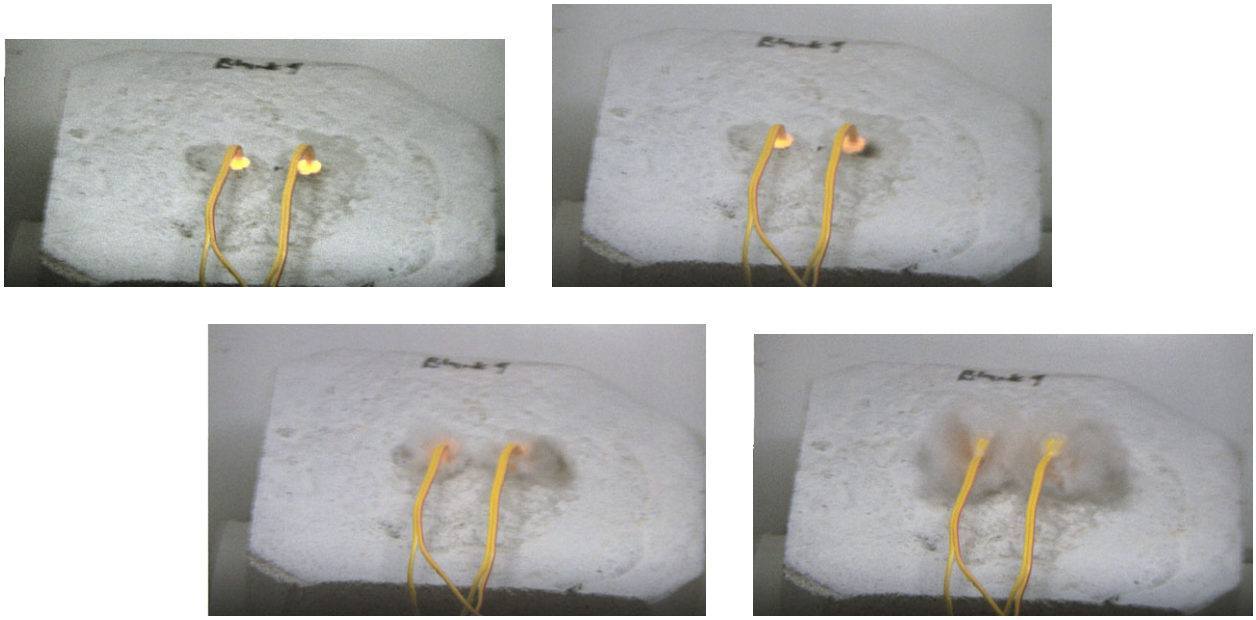

Figure 19. Selected frames from Test 4. View from left to right, and top down.

Large Block Tests

We decided to use larger samples approximately 46 x 30 x 10 cm (18 x 12 x 4 in.) for the remainder of testing, utilizing QuikCrete brand "Mason Mix" with a volumetric ratio of 3.5 parts mortar mix to one part water at room temperature, as before. Lab personnel followed the same curing process and timing for the larger blocks as for the smaller, original blocks.

One change made was to paint the sides and the bottom of the blocks to allow lab personnel easier reconstruction of the blocks after each test (Figure 20).

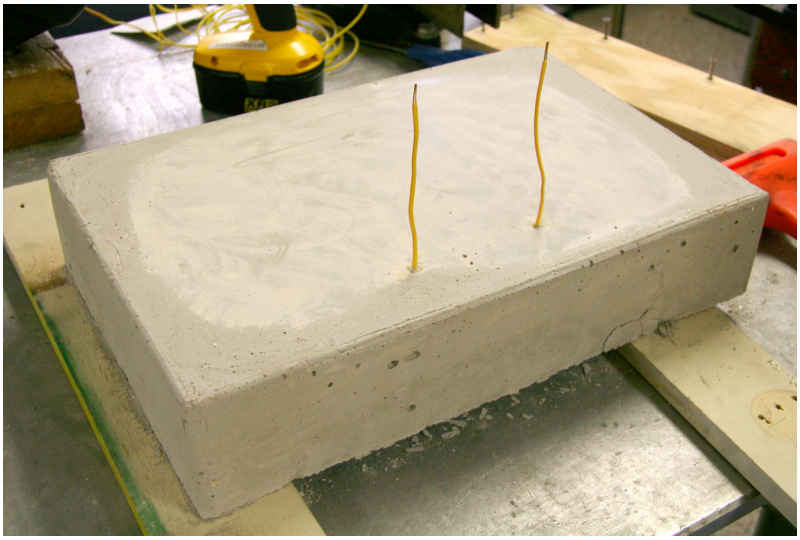

Figure 20. Test Sample 5 during surface painting to permit re-assembly of the block fragments following the shot.

Figure 21. Test Sample 5 re-assembled after the shot. Loose fragments are piled at upper right.

Test 5

The sample for this test was prepared in the same manner as the sample for Test 4, and we fired the shot in a larger atmosphere containment box that was specially designed for the larger block size. Lab personnel utilized the camera focal point discovered in our focus tests, and the camera was run at one frame/μsec. This test shot went well, but unfortunately the developer destroyed the photographic negatives and we obtained no photographic data. Lab personnel reassembled the block, however (Figure 21).

Test 6

This test was prepared and shot in the same manner as Test 5. It went well, and we utilized a different developer for our photographs. Little effect was seen in the photos of the surface of the sample until the final 2 to 3 frames. At that point, surface cracking appeared around the detonators (Figure 22). At this high frame rate, the photographs spanned only 26 μsec in time, so we decided to change the detonation time for the next sample test in order to photograph the cracking earlier in the frame sequence. We saw no spallation or other evidence of shock passage through the block. Lab personnel reassembled the block.

Test 7

The sample for this test was prepared and shot in the same manner as the samples for Tests 5 and 6, with the only change being to adjust the detonator timing so as to fire 10 μsec sooner in the frame sequence. Unfortunately, when lab personnel ran this test a problem occurred. One of the two detonators failed to fire because (as we discovered later) a firing system had become weak with age and use. Figure 23 shows the result. We saw no spallation or other evidence of shock passage through the block.

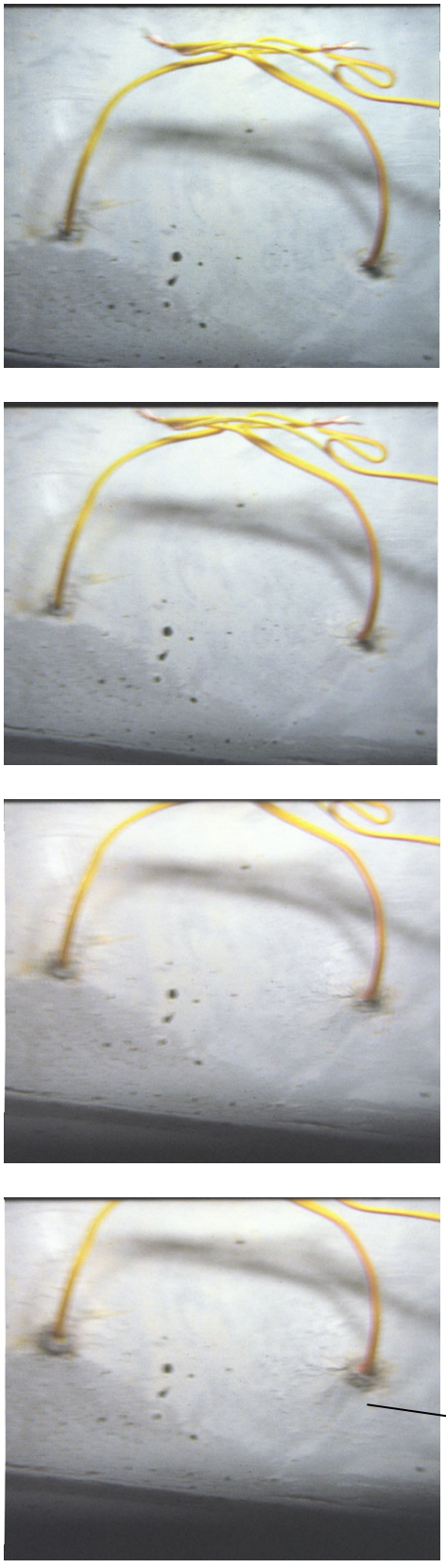

Figure 22. Selected frames from Test 6. View from top down.

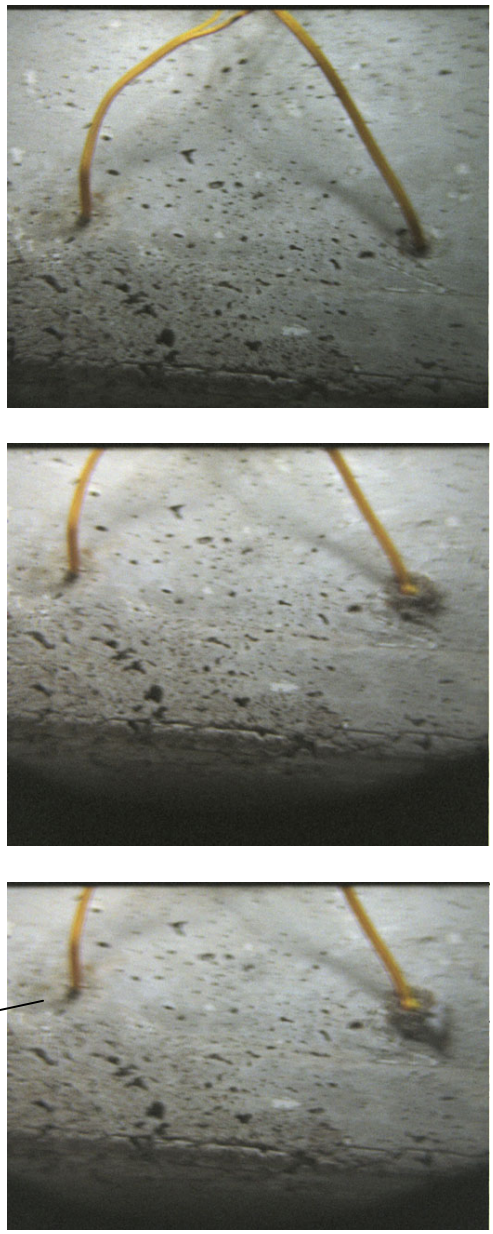

Figure 23. Selected frames from Test 7. View from top down.

Alternative Methods of Monitoring Shockwaves

Our failure to detect visually the passage of shockwaves through the mortar samples initiated a search for alternative methods to monitor the wave interactions with each other and with the rock structure. Such a method would have to have high resolution in time as well as space, and sufficient range to penetrate at least several meters into the rock at the field tests (though only a few centimeters for the laboratory shots). Unfortunately, by this point we were at the end of the period of performance. A no-cost extension was granted, but no feasible technique was found that could be exploited for this study.

One likely method would be modification of standard two- or three-dimensional sonic/seismic tomography (*c.f.* Naidu, 2001). The shockwaves themselves would be sensed by an array of geophones when the waves reach the boundaries of the test blocks. However, it is not clear how precisely such an equipment-intensive monitoring program would be able to delineate the zones of constructive and destructive interference generated by shockwave interactions if used in the standard tomographic methodologies. The P-wave velocity of the mortar from which the samples are made is 3,200 m/sec, so it takes 1.7 milliseconds for the shockwave to travel the 3.8 cm from the center of the sample to the nearest side (ignoring the top and bottom, because the shot is really a vertical line source rather than a point source). That would need sensors with resolutions of 50 kHz or more to be reasonably certain of detecting the wave passage. In addition, a dense array of transducers is needed to map the shock wave patterns in the sample blocks. It is possible that the geophones could be used as first-arrival monitors only, although this approach is limited by their expense and relatively large size with respect to the test blocks.

A related approach would be to cover the external surfaces of the test blocks with simpler, sacrificial sensors whose only task would be to react to the first arrival of the shockwave. Accomplishing this with sufficient resolution to confirm or deny the expected results would require a large number of very small and inexpensive sensors. Possibilities include simple resistive sensors, photoelectric sensors (*i.e.*, fiber optic), and photoelastic thin films. Plexiglas also was suggested as a test medium to improve internal visibility. The most likely possibility, given the difficulties experienced in this study with visual monitoring, would be the resistive or the photoelectric sensors. The total resistivity of a wire would change when the wire end is destroyed by the shockwave arrival. Its sensitivity would be controllable by adjusting the ratio of free length of the wire to embedded length, subject to the need to keep the embedded length as short as possible. It may be possible that the ends of wires could be embedded in the block surface at spacings of a few millimeters to provide the needed resolution, but it is not clear how accurate the adjacent sensors would be once the shockwave came near enough to trigger the first one. Similar concerns might attach to the use of photoelectric sensors, which would simply replace an electronic signal with a photonic one. They all might be useful, but time and effort would be required to design, test, and evaluate them.

A fourth improvement might be the use of a telecentric lens, with or without digital high-speed imaging. Either could be used alone, together, or with any of the suggestions described above. The advantage of a telecentric lens is that it effectively increases the magnification depth of field (not the same as the focus depth of field), making quantitative measurements of the shockwave position possible (Luster, 2005). It does this by forcing all incoming light rays to be parallel to each other, so near objects appear the same size as objects farther away. This requires that the lens be larger than the objects being imaged; in this case, the 101 cm by 76 cm surface of the mortar block. Additional light-gathering power is required to be able to stop the lens down

so its focus depth of field is approximately the same as its magnification depth of field. The larger the lens, however, the greater its cost.

Digital imaging, if done at the same frame rate as the Cordin camera used in this study (0.5M to 1.0M frames per second), would be more amenable to secure storage and image enhancement techniques than the analog film that it currently uses, by eliminating the requirement to send the film to an external processor. Again, the cost of digital imaging systems that can handle the extremely high frame rates required for blast imaging is rather high.

Of the several possibilities for monitoring the shockwave interference patterns in small blocks and field-scale rock masses, the most likely to be feasible remain those that rely on visual means. This is due to the high resolution required to measure the shockwave positions precisely enough to determine whether they are interacting as expected (see the next section). While standard ultrasonic transducers, for example, are perhaps more certain to detect the shockwave arrival at the block surface, the much greater size of those sensors than a pixel (even from digitized analog film) reduces the spatial resolution of the technique by about an order of magnitude. More effective methods of ultra-smoothing the surface may be of assistance, as well.

Simulation of Shockwave Interactions

In concert with the expected shockwave interactions measured from high-speed film, we explored their ideal geometry analytically and numerically. To this end we performed basic numerical calculations and graphically constructed hypothetical two-dimensional shockwave interference in a continuous, homogeneous, isotropic medium. Plots of the two types of pattern formulation served to check each other. Figures 24 through 28 result from these efforts, and concentrate on simple layouts of three to six charges.

The phase difference between two shots (or two delays) is a function of the time interval between detonations, the physical spacing between the shots, and the material properties of the surrounding medium. In rock blasting, the blast engineer has more control of the delay and the shot spacing than of the material properties. Those must be taken as they are given. To successfully apply the phased array approach to blasting, those material properties must be well-understood. One of the requirements of widespread use of this approach will be easy, cheap, high-resolution mapping of physical property variations within the target rock mass, especially porosity, density, stiffness, and tensile strength. Since rock is never a truly continuous medium, such characterization must take into account the pertinent properties of the joints, fractures, faults, cracks, and other voids. Their effect on the design of a phased array blast is the focus of a planned future study.

Constructive interference vectors are the loci of 360º (2π) phase differences between two selected shockwaves, going from the first contact between the wave crests (t=0) to a time when the summed energy of the two waves decreases to 1% of its initial magnitude ($t_{0.01}$). Note that the vectors shown in the plots below often start at a time slightly after first contact.

Figures 24 through 26 examine the shockwave interference patterns of three shots (either point or column charges – the difference would matter in the third, perpendicular, dimension) initiated with a physical shot spacing S. The heavier (primary) vector traces connect positive shockwave interactions from adjacent shots. The lighter (secondary) vector traces connect shockwave interactions from non-adjacent shots; they interact when farther from their sources and therefore their amplitudes are lower. Each diagram shows the interactions occurring at equal

time intervals over an arbitrary length of time, and the development of the constructive interference vectors thereby.

Figures 24 and 25 represent the two extreme cases possible for three collinear charges, respectively: no delay, and a delay corresponding exactly to the time necessary for a shockwave to travel through the rock to the next charge location. No delay corresponds in this instance to a row of shots all detonated simultaneously (Figure 24), so the phase difference consists entirely of physical spacing (S_1). As common sense suggests, the resulting positive interference vectors occur midway between the shots and extend outward, perpendicular to the row. The summed energy magnitude decays within a relatively short distance. For a delay equivalent to the transit time between adjacent shots (Figure 25), the resulting positive interference vectors are directed along the shot axis, 90º from the previous case. These vectors occur on top of each other, and thus extend much farther from the first shot than in the first case.

Figure 26 illustrates the positive interference vectors that result when the delay between charges is less than the time required for the shockwave to travel between the charges; 80%, in this case (see Figures 30 and 31 for calculated charts for the 60% and 80% cases). The vectors diverge, though less than in the case for no delays, and are symmetric about the axis of the charges. It is apparent that, as the delay between charges approaches the shockwave transit time

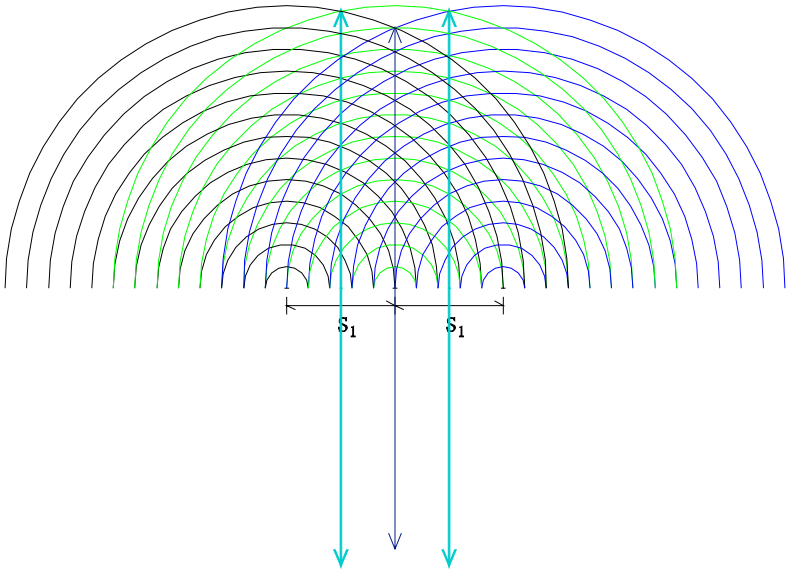

Figure 24. Constructive interference vectors for the case of no delay between three collinear point charges, extending for an arbitrary time interval following detonation and showing wavefronts at all discrete intervals calculated. For clarity, the shockwaves are shown only in a single half-space while the interference vectors are shown completely. Shockwaves from the first charge are dark blue, those from the second are light green, and those from the third are black. Vectors from positive interaction of charges one and two are light blue, those from charges two and three are dark green, and those from one and three are dark blue. Vector arrows point in the directions of propagation.

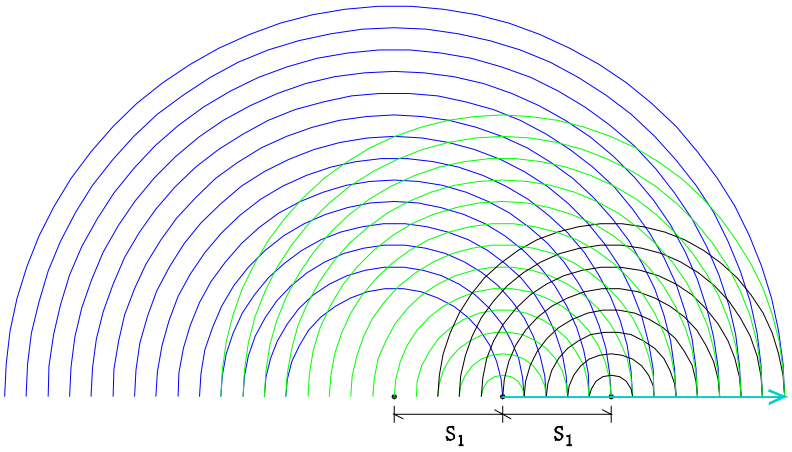

Figure 25. Constructive interference vectors for the case of 100% delay between the three collinear charges (*i.e.*, each charge fires just as the previous shockwave reaches it). See Figure 24 for explanation of graphical conventions.

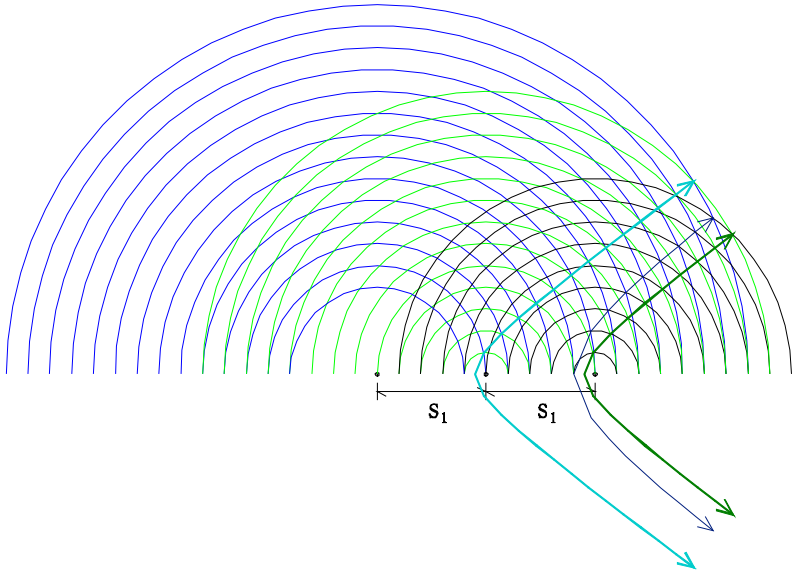

Figure 26. Constructive interference vectors for the case of 80% delay between the three collinear charges. See Figure 24 for explanation of graphical conventions.

between them, the positive interference vectors are "bent" more toward the charge axis. This relationship can be approximated by the equations:

$$\text{primary (adjacent)} \qquad \tan\alpha_P = \frac{K_P}{t_D}$$

$$\text{secondary (once-removed)} \qquad \tan\alpha_S = \frac{K_S}{t_D}$$

Where:

α	angle between vector asymptote and charge axis
t_D	transit time between charge pair (each on a different delay)
K_P	isotropic material constant (primary vector)
K_S	isotropic material constant (secondary vector)

These equations estimate the far-field directions that receive the summed energy of two shockwaves simultaneously during a multi-charge line blast. Far-field is defined as distant from the second charge by more than 30%-40% of the spacing between charges, in the direction of shockwave expansion. Primary refers to vectors generated by the interaction of adjacent charges and secondary refers to vectors generated by the interaction of alternate charges. Tertiary and lower interactions were not considered, as the shock energy would have decayed below significant levels.

However, rock blasting usually requires more complex charge geometries than lines of charges. Figures 27 and 28 illustrate the positive interference vectors produced by triangular arrays, with echelon delays.

Figure 27 shows the result when charge one fires first, charges two and four go next, and charges three, five, and six fire last. All three delays are 80% of the inter-charge transit time along the X or Y axis. Since the charges are arrayed in two dimensions, the direction along which the delay time is measured must be stated, since the distance between charges on one delay and charges on the next delay depends on direction. The minimum distance between parallel lines is along the true (perpendicular) spacing between them. In this case, the delay is equivalent to 57% of the perpendicular spacing between delays (lines of charges). The resulting interference vectors can be modeled by superimposing the case of 80% delay along each of the X- and Y-axes (Figure 26 taken twice, with one rotated 90º) onto the case of zero delay for all the charges on the same delay (Figure 24). In addition, we see the added effect of shockwaves interacting that are generated in adjacent delays, but physically offset sideways by *S*/2.

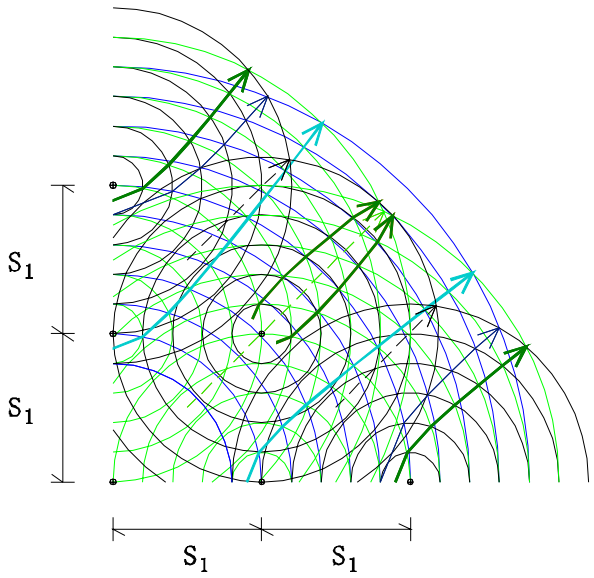

Figure 27. The case of six charges in a 2D array, fired with three delays. Each delay is, again, 80% of the physical X- or Y-distance between the shots.

Figure 28 is similar to Figure 27, but the delay in the Y-direction is 60% while the delay in the X-direction is 80%. This corresponds to a delay of 48% of the true (perpendicular) spacing between delays and would be more complex to wire in than Figure 28 since charges three, five, and six would not fire simultaneously. The delay "line" does not coincide with the physical line of charges. This skews the resulting positive interference vectors, especially in those offset patterns created when charges separated by a delay are physically offset sideways. The result is that the vectors are no longer symmetric; the more delays are included in the blast, the more they diverge from the symmetry axes evident in Figure 28.

The plots up to this point have shown all shockwaves and positive interference vectors superimposed for the duration of the blast regardless of when they actually occur, which can be difficult to decipher. To better illustrate the development of the interactions among multiple charges in a blast, Figure 29 shows the sequence of wavefronts at single timesteps for the case illustrated in summary in Figure 28. The vectors are shown in their entirety only after they have been initiated by the first contact between the shockwaves involved. This visualization shows more clearly the non-symmetric generation of the positive interference vectors for this particular case.

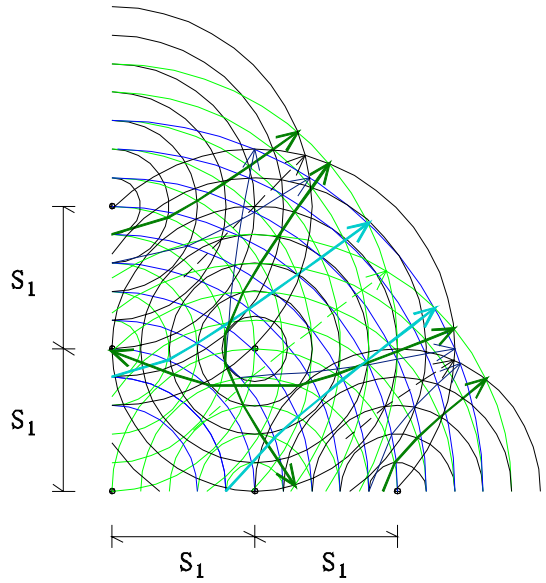

Figure 28. The case of six charges in a 2D array, fired with three delays. Each delay in the X-direction is 80% of the physical X-distance between the shots. In the Y-direction, each delay is only 60% of the physical distance. See Figure 29 for a step-by-step breakdown of the pattern.

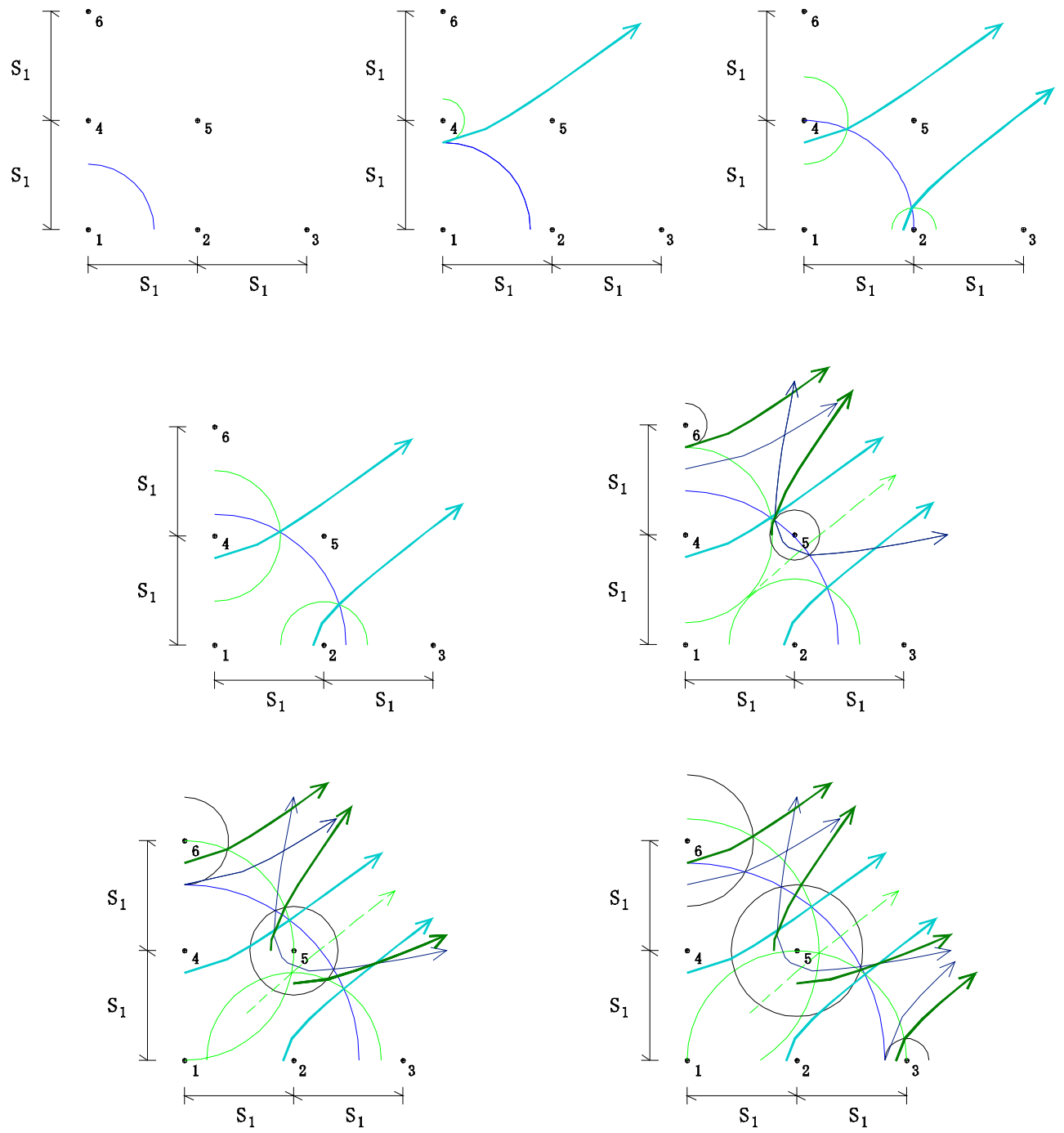

Figure 29. Individual snapshots of the graphical construction of Figure 28, which follows a constant time sequence through the shockwaves' expansion. Time increases from left to right, and from the top down (continued on the next page). See Figure 24 for color explanation.

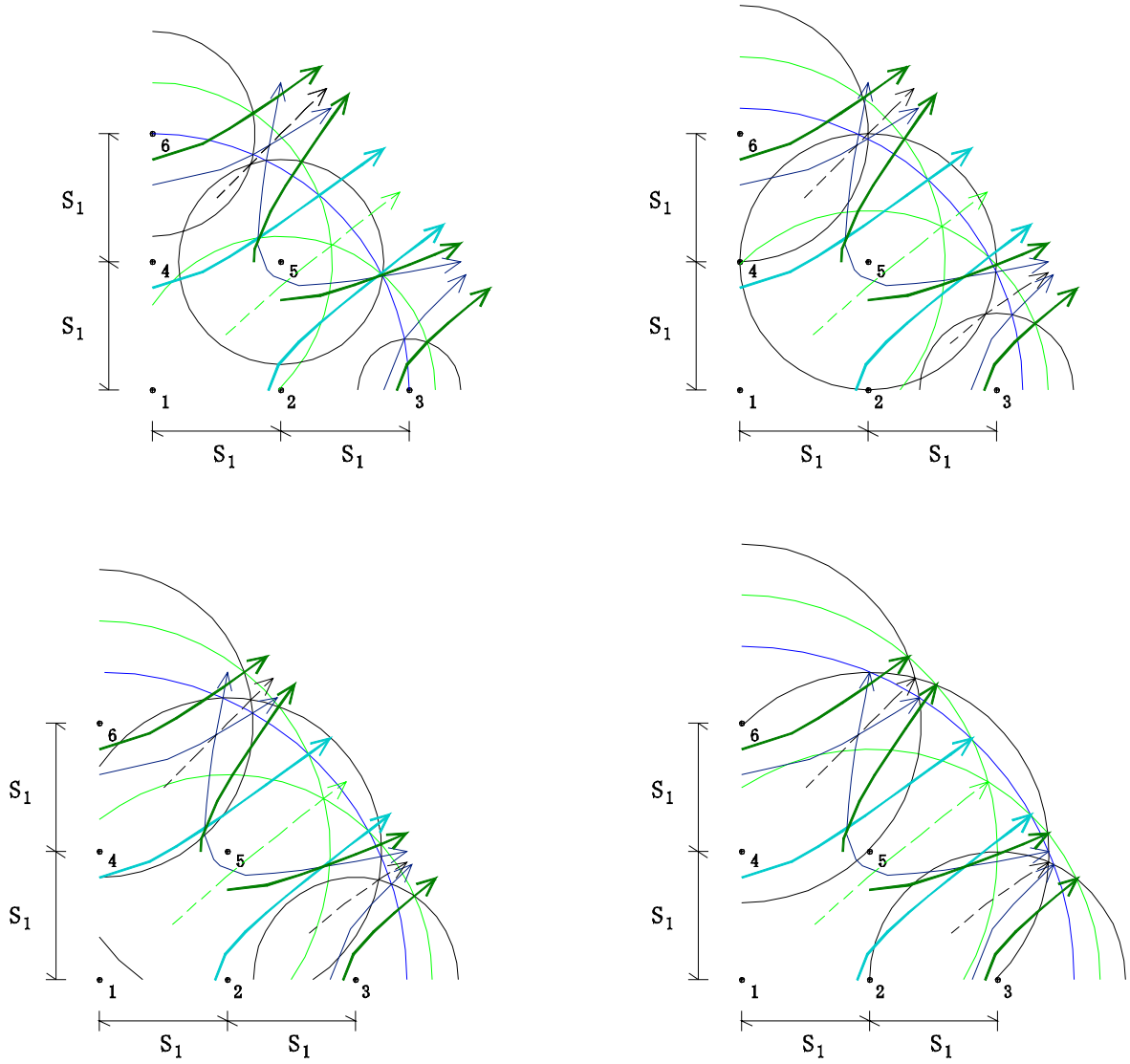

Figure 29. (Continued)

Figures 24 through 30 were generated graphically. Figures 31 through 33, which repeat the blast patterns shown in Figures 26 through 28, were generated by calculating the vectors explicitly. This was done by iteratively solving for the points shared in common by the two shockwaves in question in a sequence of timesteps. The points calculated here are arbitrary, chosen to define the curves without requiring excessive time for calculation. (The calculations and the plotting were done using MS Excel©, chosen because of its widespread accessibility and its Solver tool.) This approach permitted comparison of the positive interference vector curves to various mathematical functions; specifically, polynomials and hyperbolics.

While the general shape of the vectors is reminiscent of hyperbolic curves, these figures show that the vectors are more closely approximated by straight lines in regions far from the charges that generate them. "Far" in this case is distances greater than the spacing between charges. The

hyperbolic asymptotes (color-coded, like the linear curves, to the appropriate vector) also are not practically useful since their slopes are lower than the data points require. The linear slopes appear to be relatively accurate indicators. In the near-field, it is not clear what the most physically realistic function is; the polynomials shown are dependent on the number of points used in the fit, and are not suitable for extrapolation to the general case. Explicit calculation of discrete points may suffice for blast design in field practice, and would provide the basis for determination of a spline curve, if such precision were required. Additional study might identify useful functional approximations, as well.

The red dotted lines in the figures are isochrones. They link points on different vectors that occur simultaneously, and reveal that the primary vectors occur in advance of the secondary vectors, as would be expected since shockwaves from adjacent charges interact before the shock-waves from alternate charges do.

The spreadsheets prepared for generating these charts point the way for development of more capable blast design algorithms that can "aim" the blast energy at particular trouble spots within the rock mass, by adjusting blasthole location, delay, and charge line orientation as well as burden and spacing. With appropriate software, specific delays can be set up for each blasthole. This approach will be most easily applied to continuous, homogeneous, isotropic rock, but with practice it can be expanded to fractured, variable, and anisotropic cases as well. This is why pre-design characterization is so critical; rock variation will be the last set of constraints the engineer cannot control.

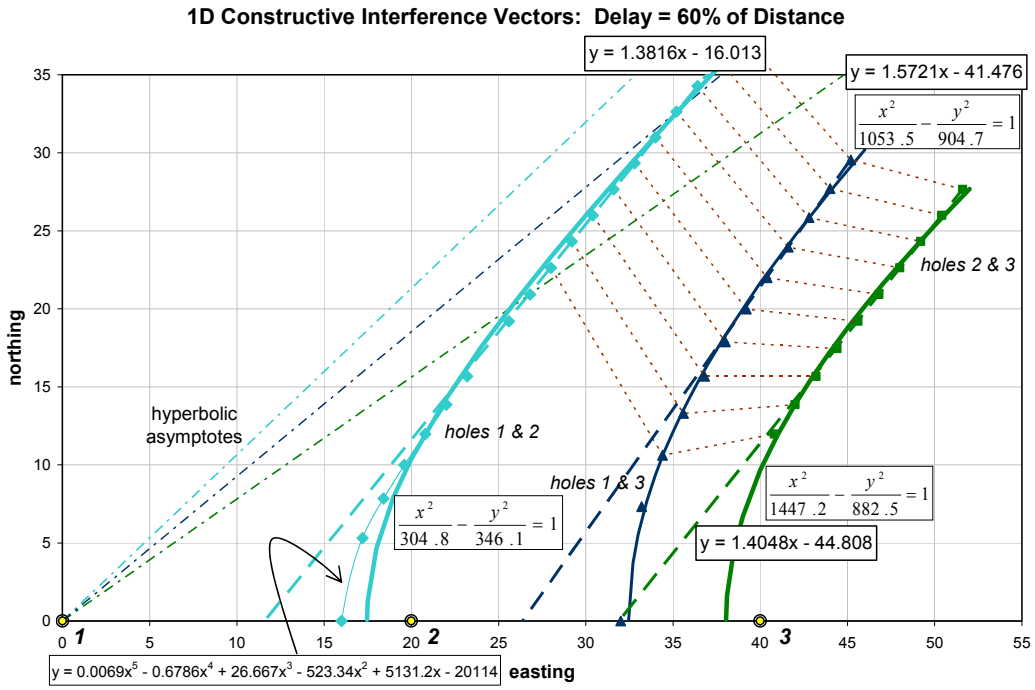

Figure 30. Calculated vectors (discrete points) and several possible curve-prediction functions for three charges, each fired when the shockwave from the previous charge had traversed 60% of the distance between them. Red dotted lines are isochrones.

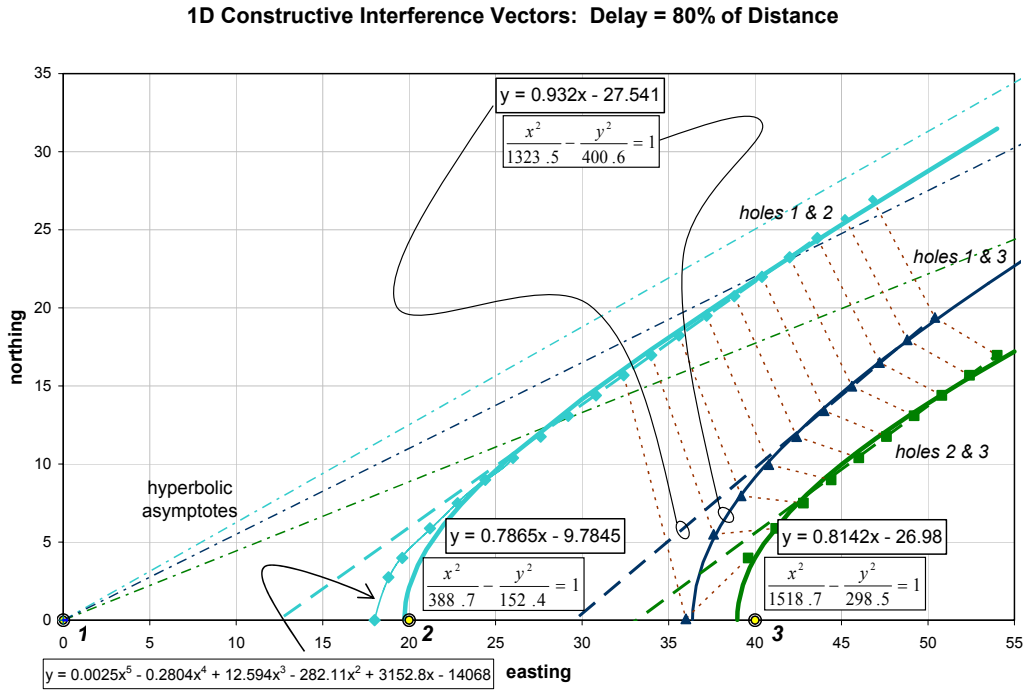

Figure 31. Calculated vectors (discrete points) and several possible curve-prediction functions for three charges, each fired when the shockwave from the previous charge had traversed 80% of the distance between them. Red dotted lines are isochrones. Compare to Figure 26.

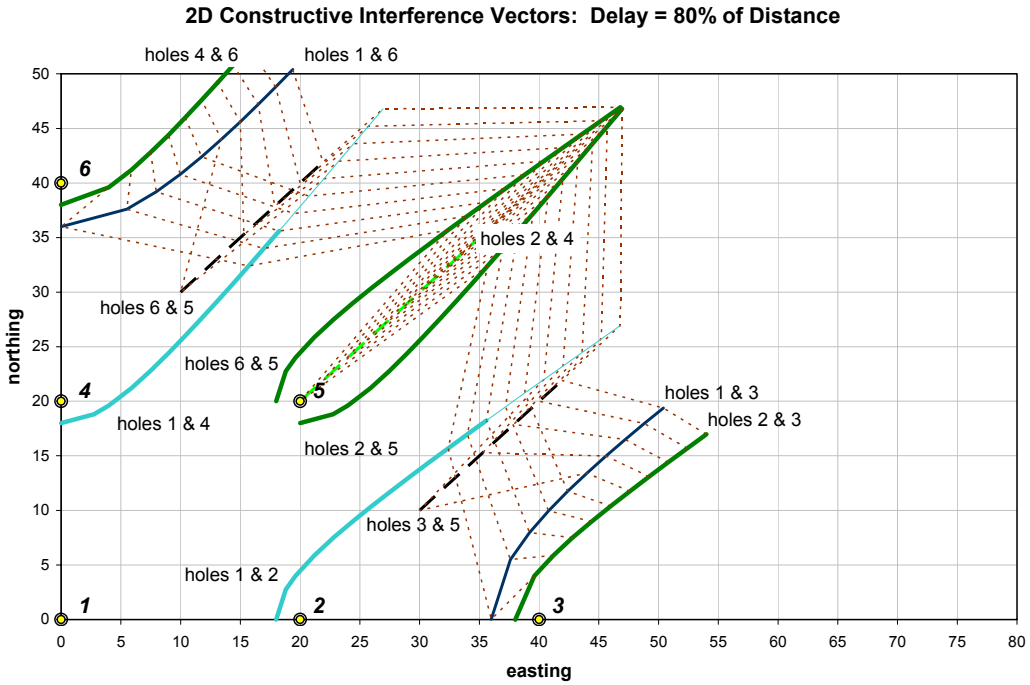

Figure 32. Calculated vectors (bold lines) and isochrones for echelon delays of six charges, timed to fire when the shockwaves have traveled 80% of the X- and Y-distances from the previous charge. Compare to Figure 27.

Potential Energy Benefits

The total energy output by a blast using a phased array approach is the same as a blast designed using standard techniques, given the same amount of explosive. However, in the phased array approach, that energy can be focused more precisely on zones where the rock fragmentability is low. In a standard-design shot, these zones would tend to produce the largest rock fragments. Therefore, the resulting fragmentation is more even, with smaller maximum fragment sizes. This provides the same effect as increasing the powder factor by 50%, calculated in Table 6. This table is extracted from Workman and Eloranta (1994) and is the basis for the Energy Savings shown in Tables 7 and 8, column two.

As a base case, we assume that taconite ore is being blasted with a heavy ANFO having absolute weight strength of 3.35 MJ/Kg (801 cal/gm). The 80% passing size of the blasted ore has been measured and found to be 40 cm (15.75 inches). The ore passes through primary and secondary crushing and grinding. The final product is 80% passing 270 mesh. Bond (1961) published a W_i for taconite of 14.87, which is used in these base case calculations.

Table 6 shows the feed and product size, the calculated total energy input, and the energy cost for each unit in the baseline operation. The explosive cost is based on an explosive cost of \$0.264/kg (\$0.12/lb). Electric energy cost is assumed to be \$0.07 per kwh.

By far the greatest work input is during grinding. Rock particle size is reduced by a factor of 360 in taconite mills. In contrast, it is reduced by a factor of four in primary crushing and by about five in secondary crushing. Clearly, changes in blasting that reduce grinding requirements will have the biggest impact on energy savings.

The second portion of Table 6 shows what occurs when the powder factor is increased to 0.45 kg/tonne (0.90 lb/ton) – the required work input has decreased by 30%, and the total cost by 26%. The cost in crushing and grinding has been reduced by 30%. No consideration was given in this analysis to increased production, less wear, or increased undersize bypassing crusher stages, but these would tend to increase the energy savings.

The energy consumed can change in three ways. First, when the feed size to the primary crusher is decreased, less energy is required to crush the ore to the same product size. Second, a decrease in W_i is related to additional fracturing and microfracturing within individual fragments. Third, there is an increased percentage of undersize fragments that bypasses stages of crushing, thereby decreasing the percentage of total tons crushed. Table 6 shows that simply increasing explosive powder factor by 36% results in a savings of 30% in work input and 26% in energy cost at today's prices.

Given current blasting practice, powder factor cannot be much increased without some means of insuring that the added energy is not lost to increased vibration. This assurance can be supplied by manipulation of shock and gas expansion energy via the use of the phased array approach; ample evidence exists in recent literature for electronic detonator-based vibration control (*e.g.*, Lewis and Pereira, 2003; McKinstry *et al*, 2004). In addition, rock fragmentation efficiency improvements through precision timing will further increase the energy savings realized by mining operations implementing phased-array blasting to at least 30%. Lastly, the inexorable increase in energy costs already being witnessed will result in an increasing percentage of energy benefits in the future; this increase is difficult to predict, however, and is not included in the table.

Tables 7 and 8 show what effect such increases in blast efficiency would have, if applied immediately throughout the U.S. mineral extraction industry. Table 7 assumes that all nonfuel mineral commodities are able to realize these savings. Table 8 applies it to only the iron mining and milling sector.

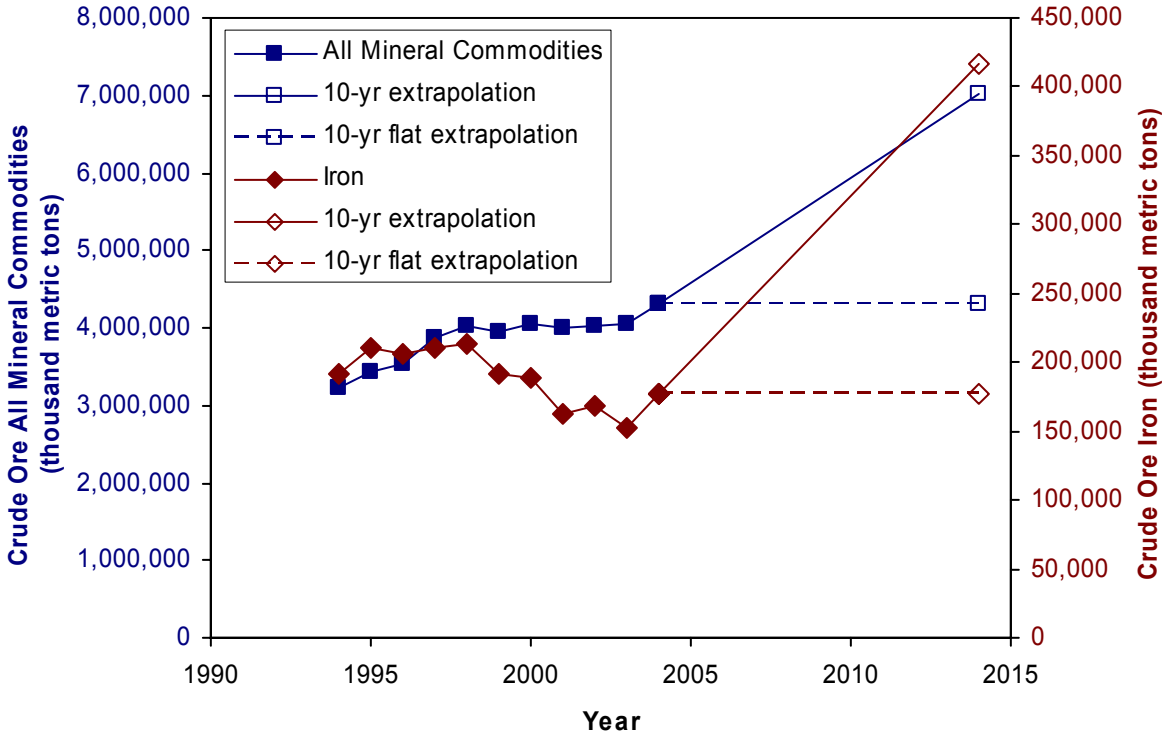

Figure 1. Forecast of current trends in surface and underground crude ore throughput for iron (red) and for all non-fuel mineral commodities (blue, metal and industrial minerals). Actual future production may be closer to the flat extrapolation than to the up-trending extrapolation. Calculated from U.S.G.S (1994-2004).

Table 6: Energy and Cost Calculations by Unit Operation (Workman and Eloranta, 2004).

Operation	Feed size, cm	Product size, cm	Work input, kWh/tonne	Energy cost, $/tonne
Explosives, powder factor = 0.33 kg/tonne	∞	40	0.24	0.087
Primary crushing	40	10.2	0.23	0.016
Secondary crushing	10.2	1.91	0.61	0.043
Grinding	1.91	0.0053	19.35	1.355

		Totals	20.43	1.413
Explosives, powder factor = 0.45 kg/tonne	∞	30	0.27	0.119
Primary crushing	30	10.2	0.135	0.009
Secondary crushing	10.2	1.91	0.428	0.030
Grinding	1.91	0.0053	13.55	0.949
		Totals	14.38	0.988

Table 7: Estimated Energy Benefits Table for All Non-Fuel Mineral Commodities.

Energy Source	Energy Savings (BTU/tonne rock) (note 1)	Future Market Penetration, additional, each year for next 8 years (tonnes/year) (note 2)	Future Energy Savings (BTU) (note 3)	Average Energy Savings (BTU/year) (note 4)
Blast-to-Mill Energy Input, electrical and explosive	2.064E+04	4.320E+06	8.024E+11	8.916E+10

Note 1: One kilowatt-hr (kWh) is equivalent to 3,413 British thermal units (BTU). The difference between the total energy required using a powder factor of 0.33 and a powder factor of 0.45 is 6.047 kWh per tonne of rock.

Note 2: Projected year 2014 production from Figure 1, using flat extrapolation. This is considered more realistic than projecting forward ten years the upward trend from 2003 to 2004.

Note 3: Summed over years 2006 through 2014.

Note 4: Average savings for each of the years 2006 through 2014, if implemented immediately.

Table 8: Estimated Energy Benefits Table for Iron Mining and Milling.

Energy Source	Energy Savings (BTU/tonne rock) (note 1)	Future Market Penetration, additional, each year for next 8 years (tonnes/year) (note 2)	Future Energy Savings (BTU) (note 3)	Average Energy Savings (BTU/year) (note 4)
Blast-to-Mill Energy Input, electrical and explosive	2.064E+04	1.770E+05	5.437E+9	6.041E+8
See Table 7 for Notes.				

Conclusion

The principle of Phased Array Blasting still appears to have great potential for improving rock fragmentation and thereby energy efficiency in mining and excavation. Although our laboratory-scale blasting tests were unable to show shockwave interactions in the mortar samples, a variety of alternative monitoring techniques was identified for future research, in both the laboratory and the field. In addition, graphical and numerical development of the interference patterns that can be expected in ideal media have revealed how to "aim" the explosive energy of a blast in cases of multiple collinear shots and in two-dimensional arrays of blastholes. These algorithms could easily be expanded to provide a tool for blast design that would enable the selection of delays on a charge-by-charge basis. The key to implementation of phased array blasting is thorough, precise, and accurate knowledge of the spatial variation of the physical properties of the target rock mass. This will be the greatest hurdle to overcome.

In future, we recommend full-scale blasting experiments (after remedying the problems experienced in this study) and also exploring the geometry of these interactions in more complex blasting situations. The ability to incorporate the effects of favorable and non-favorable orientations with respect to common geologic structures also must be developed.

Shockwaves have always interacted, focusing energy in some directions and losing it in others, but cap scatter made using it difficult. The potential of the phased array approach to rock blasting to reduce the energy usage in mineral extraction is very large, because it will bring a much greater level of control to the blasting engineer.

References Cited

American Society for Testing and Materials, 2000. "Standard Test Method for Laboratory Determination of Pulse Velocities and Ultrasonic Elastic Constants of Rock," ASTM D2845-00, ASTM International, 100 Barr Harbor Drive, PO Box C700, West Conshohocken, PA 19428-2959, United States.

Bond, F. C. 1952, "The Third Theory of Comminution," Mining Engineering, May pp 484-494.

Bond, F. C., 1961, "Crushing and Grinding Calculations," Part II, British Chemical Engineering, Aug.

Chiang, Chih-Hung and Po-Chih Chen, 2001. "Semi-direct measurements of ultrasonic pulse velocity in proposed concrete reference specimens," 10th Asia-Pacific Conference on Non-Destructive Testing, 17-21 September 2001, Brisbane, Australia, http://www.ndt.net/article/apcndt01/papers/1207/1207.htm, accessed 2 March 06.

Cook, M., 1974, The Science of Industrial Explosives, IRECO Chemicals, pp. 395-409.

Cunningham, C. "Electronic Detonators: Growing Success in Transforming Rockbreaking." Proceedings of the 30th Annual Conference on Explosives & Blasting Technique, International Society of Explosives Engineers, New Orleans, LA USA. 1-4 Feb 2004.

Eloranta, J., 1995, The Selection of Powder Factor in Large Diameter Blast Holes, Proc. of 21st Annual Conf. on Explosives and Blasting Research, Vol 1, Nashville, TN, pp 68-77.

Feldman, R.F., 1977. "Non-Destructive Testing of Concrete," Canadian Building Digest 187 (CBD-187), National Research Council Canada, Institute for Research in Construction, http://irc.nrc-cnrc.gc.ca/pubs/cbd/cbd187_e.html, accessed 2 March 2006.

Hukki, R. T., 1975, The Principles of Comminution: an Analytical Summary, Engineering and Mining Journal, Vol 176, pp 106-110.

Kawahigashi, Tatsuo, 2001. "Deterioration mechanism and estimation of durability of reinforced concrete in marine environment - 5-year exposure," Annual Reports by Research Institute for Science and Technology, Vol. 13, published by Research Institute for Science and Technology, Kinki University, Kowakae, Higashi-Osaka 577-8502, Japan, http://www.rist.kindai.ac.jp/no.13/kawah.pdf, accessed 2 March 2006.

Leslie, J.R. and W.J. Cheeseman, 1949. "An ultrasonic method for studying deterioration and cracking in concrete structures," Amer. Concrete Inst., Proceedings, Vol. 46, Sept. 1949, p. 17-36.

Lewis, N., P. Pereira. "Operating Improvements at Vulcan Materials McCook Quarry Using Electronic Detonators." Proceedings of the 29th Annual Conference on Explosives & Blasting Technique, International Society of Explosives Engineers, Nashville, TN USA. 2-5 Feb 2003.

Luster, Spencer, 2005. ""Vision Systems Design - Using telecentric lenses in inspection systems," *Vision Systems Design*, January, http://vsd.pennnet.com/Articles/Article_Display.cfm?Section=Articles&Subsection=Display&ARTICLE_ID=219446, accessed: 3 Aug 06.

McKinstry, R., T. Bolles, and M. Rantapaa, 2004, "Implementation of Electronic Detonators at Barrick Goldstrike Mines, Inc.," Proc. of 30th Annual Conf. on Explosives and Blasting Techniques, New Orleans, LA.

Mueller, Bernd and Robert Boehnke, 2004. "A New Method for the Prediction of Blast Vibrations and Suggestions with Respect to Uniform Reference Values for Short-Time Vibrations," International Society of Explosives Engineers 2004G Volume 2.

Naidu, Prabhakar S., 2001. Sensor Array Signal Processing, Boca Raton, FL: CRC Press, 458 p.

Paley, N. and Kojovic, T., 2001, Adjusting Blasting to Increase SAG Mill Throughput at the Red Dog Mine, Proc of 27th Annual Conf. On Explosives and Blasting Research, Orlando, FL.

Persson, P., 1994, Rock Blasting and Explosives Engineering, CRC Press, pp.233-250.

Reinhardt, H.W. and C.U. Grosse, 1996. "Setting and hardening of concrete continuously monitored by elastic waves," published by NDTnet, July 1996, Vol.1 No.07, http://www.ndt.net/article/grosse1/grosse1.htm and http://www.iwb.uni-stuttgart.de/grosse/papers/Frisch/frisch1.htm, accessed 1 March 2006.

Rösch, A., B. Hillemeier, E. Porzig, M. Krause, and C. Maierhofer, 1993. "Air Voids, Poor Compaction and Areas of Low Concrete Strength Detection in Concrete by Pulse Velocity Measurement," http://beta.bv.tu-berlin.de/forsch/roesch/column.htm, accessed 2 March 2006.

Rosenstock, W. "Advanced Electronic Blasting Technology, ABET: Breaking 3,205,000 Tonnes of Ore Within a Millisecond." Proceedings of the 30th Annual Conference on Explosives & Blasting Technique, International Society of Explosives Engineers, New Orleans, LA USA. 1-4 Feb 2004.

Rossmanith, H.P, 2003a, "The Mechanics and Physics of Electronic Blasting." Proceedings of the 29th Annual Conference on Explosives & Blasting Technique, International Society of Explosives Engineers, Nashville, TN USA. 2-5 Feb 2003.

Rossmanith, H.P., 2003b, "The Mechanics and Physics of Electronic Blasting," International Society of Explosives Engineers 2003G, Volume 1.

Rossmanith, Hans-Peter, 2004. "What You Always Wanted to Know About Blast Waves in Blocky Benches," International Society of Explosives Engineers 2004G Volume 2.

Sames, Frank, 1995. "Vibration Controlled Blast Timing Optimization Using the Seed Waveform Modeling Concept," ISEE Sixth High Tech Seminar on Blasting Technology, Instrumentation and Explosives Applications, Boston, Massachusetts, USA, July 8 - 13, 1995.

U.S. Geological Survey, 1994-2004, "USGS Minerals Information: Mining and Quarrying," http://minerals.usgs.gov/minerals/pubs/commodity/m&q/, accessed 3 Aug 2006.

Willis, B. A., 1988, Enhancement of Mineral Liberation, Proceedings of XVI International Minerals Processing Congress, pp 293-297.

Workman, L., and J. Eloranta, 2004, "The Effects of Blasting on Crushing and Grinding Efficiency and Energy Consumption," http://www.elorantaassoc.com/propapers.htm, accessed 3 Aug 2006.